DIFFUSE IONIZED REGIONS IN THE VICINITY OF ACTIVE GALAXIES

by

ERIN KAY DARNELL

WILLIAM C. KEEL, COMMITTEE CHAIR

RAYMOND WHITE
JIMMY IRWIN
D. MICHAEL CRENSHAW

A THESIS

Submitted in partial fulfillment of the requirements
for the degree of Master of Science in the
Department of Physics and Astronomy
in the Graduate School of
The University of Alabama

TUSCALOOSA, ALABAMA

2011

Copyright Erin Kay Darnell 2011
ALL RIGHTS RESERVED

ABSTRACT

Using a sample of 37 Active Galactic Nuclei (AGN), we investigated the incidence of giant ionized clouds in the vicinity of active galaxies. We carried out remote observations of the sample using the Southeastern Association for Research in Astronomy (SARA) North telescope at Kitt Peak and the SARA South telescope on Cerro Tololo. Frames were taken in continuum V and using a narrowband filter that transmits redshifted [O III] λ5007. We formed an emission line image by subtracting the combined and scaled V frames from the combined [O III]-line frames. To reduce uncorrelated noise, the emission line images are median filtered with a 1".9 x 1".9 box size. To bring out large diffuse regions, we convolve the images with a circular Gaussian function of 3".42 FWHM. Emergent structures are determined to be starlight or ionized gas. 20 members of our sample were recently shown to be tidally disrupted in an atomic Hydrogen (HI) study. No extended [O III]-line emission clouds were seen in the vicinity of any from this group. We found one new instance of extended ionized emission clouds near the Seyfert 1 galaxy RX J1103.2-0654.

LIST OF ABBREVIATIONS AND SYMBOLS

AGN	Active Galactic Nuclei
NED	NASA/IPAC Extragalactic Database
SARA	Southeastern Association for Research in Astronomy
IRAF	Image Reduction and Analysis Facility
α or RA	Right Ascension
δ or Dec	Declination
CCD	Charge Coupled Device
VCV	Veron-Cetty Veron
(k)pc	(kilo)parsec
SDSS	Sloan Digital Sky Survey
MCG	Morphological Catalogue of Galaxies
IC	Index Catalogue
UGC	Uppsala General Catalog of Galaxies
NGC	New General Catalogue (of Nebulae and Star Clusters)
CBH	Central Black Hole
ISM	Interstellar Medium
FOV	Field of View
RD	Residual Dark
ELI	Emission Line Image
ZP	Zero Point
$A_{N\,or\,S}$	Collecting Area of the SARA-N or SARA-S Telescope
HI	Atomic Hydrogen

ACKNOWLEDGMENTS

I would like to thank Bill Keel for the many hours spent guiding me through the details of remote observing and data reduction, and for the patience with which he has introduced me to AGN research. I would like to thank Raymond White for his guidance and willingness to help me organize and work towards my academic goals. I would also like to thank the members of my committee for taking the time out of their schedule to participate in this process. Last but not least I would like to thank Ryoichi Kawai and Katy Garmany, who have mentored me over many years.

CONTENTS

ABSTRACT....ii

LIST OF ABBREVIATIONS AND SYMBOLS....iii

ACKNOWLEDGMENTS....iv

LIST OF TABLES....vi

LIST OF FIGURES....vii

1. INTRODUCTION....1

a. Active Galaxies....1

b. Galaxy-Scale Diffuse Ionized Clouds....2

2. OBSERVATIONS AND SAMPLE SELECTION....5

a. Observing with the SARA Telescopes....5

b. The Sample....6

3. REDUCTIONS AND MEASUREMENTS....9

a. Data Reduction....9

b. Image Alignment, Combination, Scaling and Subtraction....9

c. Calibration 11

4. IMAGES....13

5. RESULTS AND DISCUSSION....34

REFERENCES....36

LIST OF TABLES

1. The Active Galaxy Sample.....7

2. The Active Galaxy Sample from Kuo, et. al. 2008.....8

3. Observing Information for Landolt Standards.....11

4. Table 4.....33

LIST OF FIGURES

1. Voorwerp Spectrum....3
2. f510 and V Transmission Curves....5
3. Illustration of RD Afterglow Correction....10
4. Example of an Image Set....13
5. MARK 341....14
6. Mrk 352....14
7. Mrk 1....15
8. NGC 513....15
9. Mrk 993....16
10. Mrk 359....16
11. UGC 1395....17
12. NGC 841....17
13. Mrk 1040....18
14. NGC 973....18
15. NGC 1167....19
16. UGC 3157....19
17. MS 04595+0327....20
18. 2E 0507+1626....20
19. MCG -04.16.001....21
20. UGC 3478....21

21. UGC 3995.....22

22. NGC 2639.....22

23. NGC 2824.....23

24. MCG -01.24.012.....23

25. Mrk 1419.....24

26. RXS J11032-0654.....24

27. NGC 3822.....25

28. NGC 4404.....25

29. NGC 4619.....26

30. 3C 278.....26

31. Mrk 461.....27

32. IRAS 14082+1347.....27

33. Mrk 1510.....28

34. NGC 5548.....28

35. Zw 338.014.....29

36. NGC 6240.....29

37. Ark 539.....30

38. UGC 11630.....30

39. NGC 7469.....31

40. IC 1515.....31

41. ESO 602- G25.....31

42. NGC 7679.....32

43. NGC 7682.....32

44. RX J1103.2-0654.....34

I. INTRODUCTION

a. Active Galaxies

An active galactic nucleus refers to the existence of a strong non-stellar source of radiation in the central region of a galaxy. Active Galactic Nuclei (AGN) embody some of the most extreme conditions found anywhere and include the most powerful individual objects in the known Universe. They are characterized by high luminosity and continuum radiation over a broad range of wavelengths, with rapid variability on time scales of days or even hours. They exhibit a strong UV excess, unusually blue colors, and emission lines with significant widths [10]. At the center of all galaxies there is a massive compact object [21, 20], commonly thought to be a central black hole (CBH) [16]. Accretion onto a CBH is the most plausible power source for AGN, though details of the source or origin of this material are still an unresolved topic in AGN research. The demography of massive dark objects in galaxy centers is roughly consistent with the hypothesis that these are dormant AGN [3].

The first optical spectrum of an active galaxy was obtained at Lick Observatory in 1908 by E.A. Fath as part of his dissertation work [6]. He noted the presence of strong emission lines in the "nebula" NCG 1068. A few years later, from Lowell Observatory, V.M. Slipher was able to resolve these lines and found widths over a thousand km s^{-1} [25]. The first class of AGN was identified by Carl Seyfert in 1943 [24]. He presented 6 extragalactic nebulae (spiral galaxies) having high central surface brightness with nuclei producing spectral signatures of highly ionized gas. Historically, Seyferts have been classified based on their optical spectra, with Seyfert 1s possessing broad permitted lines, narrower forbidden lines and non-stellar continua. Seyfert 2s have permitted and forbidden lines of similar widths and the host galaxy

dominates the optical continua [11]. Other types are given a fractional classification going from 1.0 to 2.0 depending on the relative broadness of the emission lines. Inspired by the discovery of polarized broad permitted lines and continua not attributed to host galaxy in spectro-polarimetric observations of Seyfert 2s [17], Seyfert Unification Theory [1] links all Seyferts to a powerful central engine surrounded by a torus of dust and molecular gas, with the type of Seyfert seen only a matter of how our line of sight passes this torus - through the pole in S1's and through the equator in S2's. About 10% of all Sa and Sb spirals have Seyfert nuclei.

The most luminous class of AGN are the quasars, which can outshine their host galaxies by 2 orders of magnitude [12]. In the 1950's, radio surveys such as the Third Cambridge Catalog (3C) and Parkes Survey of Southern Hemisphere (PKS) began finding quasi-stellar radio sources. These objects emitted very strong optical and radio signals from an apparently point-like source. At Palomar Observatory in 1963, Maarten Schmidt resolved the mystery of these "galactic stars" with peculiar spectra when he realized that broad lines in the quasar 3C 273 were very redshifted nebular lines [23]. Many similar objects that are not strong radio sources (QSOs) are now also included in the quasar category; the current estimate is that 5-10% of AGNs are radio loud.

Galaxy formation is significantly modulated by energy output from the CBH. There are indications that a CBH transitions in and out of highly efficient luminous quasar phases but the timescale for this transition has been elusive.

b. Galaxy Scale Diffuse Ionized Clouds

While the central engines of AGN can not be observed directly, emission-line structures can be large and well-resolved, particularly those we are looking for which are several (10-100) kpc from the AGN. AGN-ionized clouds can be used to probe central engine properties: Opening angle over which ionized radiation escapes can be inferred and used to check how the viewing angle determines the degree of obscuration by the dusty torus thought to surround the CBH; The calculated light travel time to the cloud and then us can provide a view to

the immediate past of the AGN [5, 28].

In 2007, a Galaxy Zoo [15] volunteer named Hanny van Arkel reported an unusual object near the spiral galaxy IC 2497 [14]. Known today as Hanny's Voorwerp, this cloud of ionized gas is the progenitor of our survey. Detailed multi-wavelength studies of the Voorwerp found that it contains highly ionized gas with line ratios similar to extended emission-line regions near luminous AGN, despite no apparent ionization source (Figure 1).

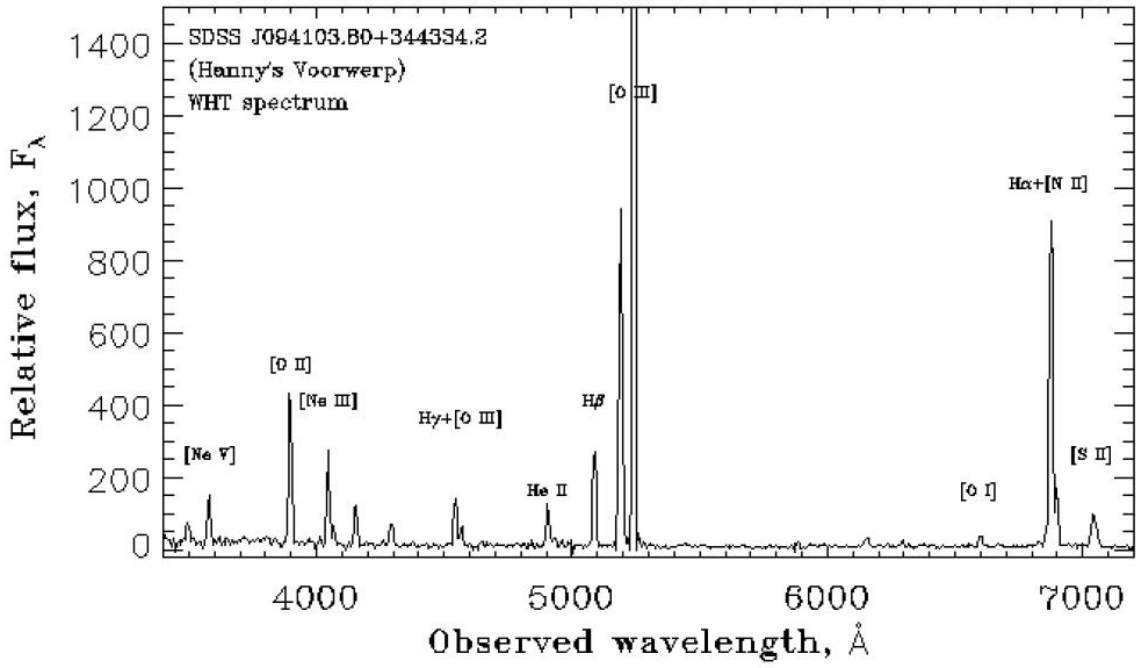

Figure 1: Voorwerp Spectrum. WHT Composite Spectrum Plot of an extended emission-line cloud.

The hypothesis now is that the Voorwerp may be a quasar light echo, an indicator of quasar history that can trace a sudden and dramatic decrease in the luminosity of the nearby galaxy's central source [14]. Kevin Schawinski et al. 2010 [22] determined that the extremely rapid shutdown of IC 2497's central engine quasar occurred within the past 70,000 years. This may signal a transition of the accretion disk to a radiatively inefficient state where the bulk of the energy is dissipated as thermal or kinetic energy [2, 18] and could be due to a sharp decrease in the fuel supply or a change of accretion state. Followup studies on extended emission line regions from a more recent Galaxy Zoo survey confirmed 19 more AGN-ionized

gas clouds from which the duration of luminous episodic activity of AGN in Seyfert galaxies was calculated to be 0.2-2x10^5 [28]. At least 14/19 of these were found in interacting or merging systems, supporting earlier evidence [19, 9] that these clouds may be illuminated tidal debris. A 2008 HI study of Seyferts [13] showed that while only 16% showed optical disturbance, most (94%) are disturbed in atomic Hydrogen gas (HI). With HI being the most enduring and sensitive tracer known of tidal interactions, and with tidal tails thought to be a prime source of distant gas out of the galaxy plane to be ionized by AGN, we are observing all AGN in this sample. For any with extended ionized emission clouds, a structure comparison to the HI map could yield detailed tests of the Seyfert unified model in addition to usual information gained from cloud properties. Other types of extended emission line regions have been studied around luminous AGN, especially around radio-loud galaxies [26, 7].

2. OBSERVATIONS AND SAMPLE SELECTION

a. Observing with the SARA Telescopes

We collected data using two remotely operated telescopes of the Southeastern Association for Research in Astronomy (SARA). SARA-N is a 914 mm telescope sited at Kitt Peak National Observatory in Arizona. Its detector is a 2048x2048 pixel E2V chip in an Apogee U42 camera. The EG gain is 1.2 electrons per count and readout noise is 6.3 electrons. The field of view (FOV) is around 12' x 12' with a pixel sampling of 0.38 arcsec pix^{-1}. This is an appropriate size for our survey. SARA-S is a 609.6 mm telescope located on the south-east ridge of Cerro Tololo in Chile. It's detector is an Apogee Alta E6. The FOV of is around 10' x 10' with the angular size of a pixel 0.606 arcsec pix^{-1}.

Observations occurred over 20 nights, beginning in September 2010. Biases, darks, and V & f510 twilight sky flats were usually taken at the beginning of the night. A peculiar property of our chip is that very bright objects can leave an afterglow [4]. To protect against false detections due to this, we offset the telescope ~60" of declination between frames. We commonly took a 5-10 minute "residual" dark (RD) when moving between galaxies for use in the reduction process to further protect against afterglow effects. Our goal was a total f510/10 exposure time of 5400 seconds and a total V band exposure of 1800s, though this was not always achieved. We took several shorter exposures, slightly offsetting the telescope between each as mentioned above, and later combined them. Doing so reduced cosmic ray contamination without compromising depth of view and sampling the object at different locations on the chip let us effectively average out some of the small-scale flat fielding errors. At SARA-N, the sky-noise dominates over readout noise for sky levels greater than $\frac{6.3^2}{1.2} = 34$ ADU which was always met so we achieved the same sensitivity with this method as with

one long exposure.

All of our [O III]-line observations had to be done with the SARA-N telescope at Kitt Peak where the λ510/10 filter resides, and most of our V data was gathered there as well. Both telescopes have the standard UBVR filters.

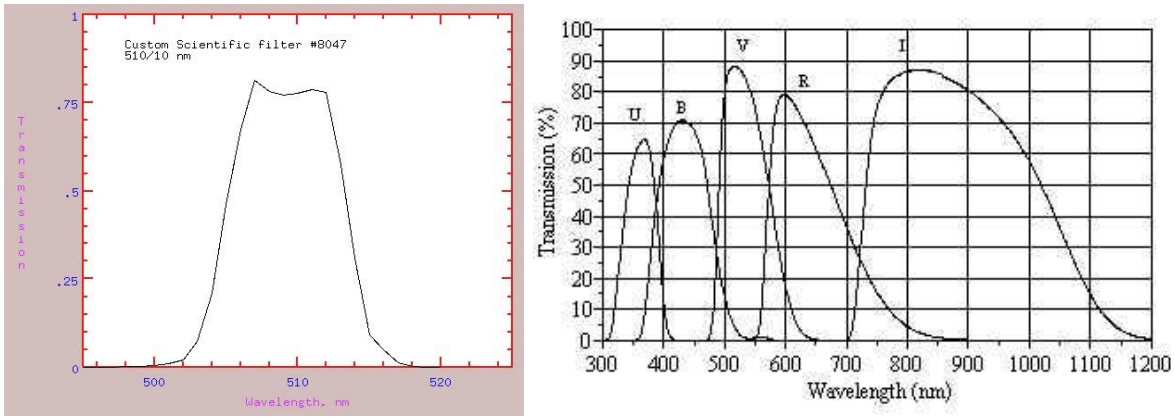

Figure 2: f510 and V transmission curves. f510 filter at SARA-N is on the left, UBVRI filters on right.

We used the [O III] emission line at 5007 Å for our search. The spectrum of Hanny's Voorwerp is typical of extended emission clouds like those we seek, so Figure 1 shows why this emission line is the best choice. To use the λ510/10 filter (f510) to look for [O III] λ5007, our sample of galaxies required redshifts (z= $\frac{\lambda_o}{\lambda_e}$-1) within a range such that the filter captured this line close to the peak. As Figure 2 shows, f510 has half transmissions points at 5040 Å and 5135 Å, corresponding to a redshift range of z=0.00659 to z=0.0256. 5007 Å falls close to the center (about 45 nm to the red) of the V band, which we used for deep continuum imaging.

b. The Sample

We queried the Veron-Cetty & Veron catalog [27] of AGN for galaxies meeting our redshift criteria. 20 members of the sample presented here were selected from the most optically luminous of those returned to our query. This sample was supplemented by an additional 17 galaxies from [13], see Table 2. Information obtained from NED is also listed in Table 1.

α δ (Equinox J2000.0)	HI	Name	z	Activity Type	Mag./Filter
00h36m52.3s +23d59m06s	A	MARK 341	0.0153	Sy	14.7
00h59m53.3s +31d49m37s	rfi	Mrk 352	0.0149	Sy 1.0	14.8
01h16m07.2s +33d05m22s	A	Mrk 1	0.0159	Sy 2	15.0
01h24m26.9s +33d47m58s	B	NGC 513	0.0195	Sy 1 h	13.9
01h25m31.5s +32d08m11s	C	Mrk 993	0.0155	Sy 1.5	14.4
01h27m32.6s +19d10m44s	nd	Mrk 359	0.0174	Sy	14.2
01h55m22.0s +06d36m43s	B	UGC 1395	0.0174	Sy 1.9	14.2
02h11m17.4s +37d29m50s	A	NGC 841	0.0151	LINER b	13.4
02h28m14.5s +31d18m42s	A	Mrk 1040	0.0167	Sy 1.0	14.5
02h34m20.1s +32d30m20s		NGC 973	0.0162	S2	13.6
03h01m42.4s +35d12m21s	C	NGC 1167	0.0165	LINER	13.4
04h46m29.8s +18d27m39s	C	UGC 3157	0.0154	Sy 2	15.0
05h02m09.0s +03d31m50s	B	MS 04595+0327	0.0160	Sy 1	14.8
05h10m45.5s +16d29m56s	nd	2E 0507+1626	0.0179	Sy 1.5	15.6
06h23m51.0s -23d11m37s		MCG -04.16.001	0.0240	S	14.4
06h32m47.2s +63d40m25s		UGC 3478	0.0128	S1n	13.6
07h44m09.3s +29d14m48s	C	UGC 3995	0.0158	S2	13.3
08h43m38.1s +50d12m20s		NGC 2639	0.0111	LINER	12.4
09h19m02.2s +26d16m12s		NGC 2824	0.0092	Sy ?	14.2
09h20m46.2s -08d03m22s		MCG -01.24.012	0.01964	Sy 2	15.0
09h40m36.4s +03d34m37s	C	Mrk 1419	0.0165	LINER	13.3
11h03m16.8s -06d54m17s		RXS J11032-0654	0.0261	S1	15.4
11h42m11.1s +10d16m40s		NGC 3822	0.0209	Sy 1.9	14.1
12h26m16.2s -07d40m51s		NGC 4404	0.0186	S3	13.1
12h41m44.5s +35d03m46s		NGC 4619	0.0231	Sy 1.0	13.5
14h10m41.3s +13d33m29s	C	IRAS 14082+1347	0.0162	LINER	15.0
14h17m58.7s +26d24m45s	rfi	Mrk 1510	0.0147	H II	14.1
14h17m59.5s +25d08m12s	A	NGC 5548	0.0172	Sy 1.5	13.3
15h42m55.4s +70d49m41s		Zw 338.014	0.0253	Sy ?	15.5
16h52m58.9s +02d24m03s		NGC 6240	0.0245	LINER / S3	13.8
18h28m48.1s +50d22m21s	A	Ark 539	0.0169	Sy 2	15.4
20h47m34.1s +00d24m42s		UGC 11630	0.0126	Sy 2	14.0
23h03m15.6s +08d52m26s	A	NGC 7469	0.0163	Sy 1	13.0
23h56m03.9s -00d59m19s		IC 1515	0.0222	Sy 2	14.5
22h31m25.5s -19d02m04s		ESO 602-G25	0.0250	Sy	14.0
23h28m46.7s +03d30m41s	A	NGC 7679	0.0171	Starburst	13.5
23h29m03.9s +03d32m00s	A	NGC 7682	0.0171	Sy 2	14.1

Table 1. The Active Galaxy Sample. In the HI column, A indicates strong HI disturbance due to interaction with neighboring galaxy, B designates HI disturbance not directly linked to (if any) neighboring galaxy, and C indicates no or weak HI disturbance. rfi and nd mean the galaxy was removed from analysis due to radio frequency interference or else it was not detected in HI.

ACTIVE GALAXY SAMPLE

Name	R.A. (J2000)	Decl. (J2000)	z	Spectral Type	M_B	Hubble Type	Inclination (degrees)	log $L_{[OIII]}$ (erg s^{-1})	Refs. $L_{[OIII]}$
Markarian 341	00 36 52.2	23 59 06	0.017	S	−21.9	S0-a	70.5	...	
NGC 266	00 49 48.2	32 16 43	0.015	LINER	−20.6	Sab	14.5	...	
Markarian 352	00 59 53.3	31 49 37	0.015	S1.0	−19.5	S0	33.9	40.89	2
Markarian 1	01 16 07.2	33 05 22	0.016	S2	−19.0	Sb	58.7	41.56, 41.85	1,2
NGC 513	01 24 26.8	33 47 58	0.016	S1.9	−21.5	Sc	61.9	...	
Markarian 993	01 25 31.4	32 08 11	0.017	S1.5	−20.0	Sa	90.0	40.49	1
Markarian 359	01 27 32.5	19 10 44	0.017	S1	−20.2	Sb	39.1	41.05, 41.13	1,2
Markarian 1157	01 33 31.2	35 40 05	0.015	S2	−20.1	S0-a	40.2	41.39, 41.39	1,2
Markarian 1158	01 34 59.5	35 02 22	0.015	H II	−19.3	S?	58.7	40.95	1
Markarian 573	01 43 57.8	02 20 59	0.017	S2	−20.1	S0-a	28.0	41.92, 42.30	1,2
UGC 1395	01 55 22.1	06 36 42	0.017	S1.9	−20.5	Sb	54.8	40.89	2
NGC 841	02 11 17.3	37 29 49	0.015	LINER	−21.4	Sab	64.8	...	
Markarian 1040	02 28 14.4	31 18 41	0.016	S1.0	−19.2	Sbc	81.1	40.98, 41.19	1,2
NGC 1167	03 01 42.4	35 12 21	0.016	LINER	−21.1	S0	49.0	...	
UGC 3157	04 46 29.7	18 27 40	0.016	S2	−19.9	Sbc	35.2	...	
MS 04595+0327	05 02 09.0	03 31 51	0.016	S1	−19.5	S?	50.2	...	
2E 0507+1626	05 10 45.5	16 29 56	0.017	S1.5	−19.4	E?	39.7	...	
UGC 3995	07 44 09.2	29 14 50	0.015	S2	−21.5	Sb	67.6	...	
Markarian 1419	09 40 36.5	03 34 38	0.015	LINER	−19.8	Sa	41.9	40.72	1
Markarian 461	13 47 17.7	34 08 56	0.016	S2	−20.4	Sab	43.6	...	
IRAS 14082+1347	14 10 41.7	13 33 27	0.017	LINER	−19.5	S?	53.5	...	
Markarian 1510	14 17 58.6	26 24 47	0.015	H II	−20.7	Sbc	48.2	...	
NGC 5548	14 17 59.6	25 08 13	0.017	S1.5	−20.7	S0-a	41.0	41.81, 41.91	1,2
ARK 539	18 28 48.2	50 22 22	0.016	S2	−19.9	S?	31.9	40.22	1
NGC 7469	23 03 15.6	08 52 26	0.017	S1.5	−21.6	Sa	30.2	42.00, 41.84	1,2
NGC 7591	23 18 16.3	06 35 09	0.017	S	−21.6	SBb	67.1	...	
NGC 7679	23 28 46.6	03 30 42	0.016	S2	−21.4	S0-a	59.1	...	
NGC 7682	23 29 03.9	03 32 00	0.017	S2	−20.7	Sab	22.7	41.46	2

NOTE. — Units of right ascension are hours, minutes, and seconds, and units of declination are degrees, arcminutes, and arcseconds. Spectral type S denotes unclassified Seyfert galaxy. All data apart from Hubble types and inclinations are from the Véron-Cetty & Véron (1998) catalog, except for UGC 3157 from the Véron-Cetty & Véron (2000) catalog. UGC 3995 is referred to in Véron-Cetty & Véron (1998) as UGC 3995A. Hubble types and inclinations are from the Hyperleda database, where E? and S? denote unclassified elliptical and spiral galaxies respectively. The [OIII] luminosities are computed from measurements by Dahari & de Robertis (1988) and/or Whittle (1992) assuming $H_o = 50$ km s^{-1} Mpc^{-1} and $q_0 = 0$. In the last column, reference 1 refers to Dahari & de Robertis (1988) and refrence 2 to Whittle (1992).

Table 2: The Active Galaxy Sample from Kuo, et. al. 2008[13]. [O III] luminosities are for the nucleus.

3. REDUCTIONS AND MEASUREMENTS

a. Data Reduction

IRAF was used to carry out standard data reduction techniques. For each night, bias frames were combined to give us a zero image that was subtracted from all of the other images. Darks were combined by exposure time and subtracted from our sky flats and science images with corresponding exposure times. Then filter-specific flats were combined and normalized to 1. These were divided out of the science images to complete the initial data reduction procedure. When applied, our residual darks (RDs) were zero and dark subtracted, median filtered, scaled, and then subtracted from the science images. Figure 3 illustrates RD correction.

b. Image alignment, combination, scaling and subtraction

Radial profiles of 5-20 stars per image were determined by IRAF's **imexamine** task, which also gave the star's physical coordinates. Images of a common galaxy were aligned by calculating and applying the shift between these stars. For each filter, the standard **imcombine** task was used to combine the aligned images using a median profile and 'sigclip' rejection operation. With n~3 exposures, we used small sigma clipping factors of 1.5 to reject outliers. The resulting images gave continuum V and redshifted-[O III] data. We zeroed the background sky in these combined images. We again examined the radial profile of 6-20 stars in each image to determine the (v/o3) count ratio. This hinted at an appropriate scaling factor for the v image such that its subtraction from o3 would result in mostly blank sky.

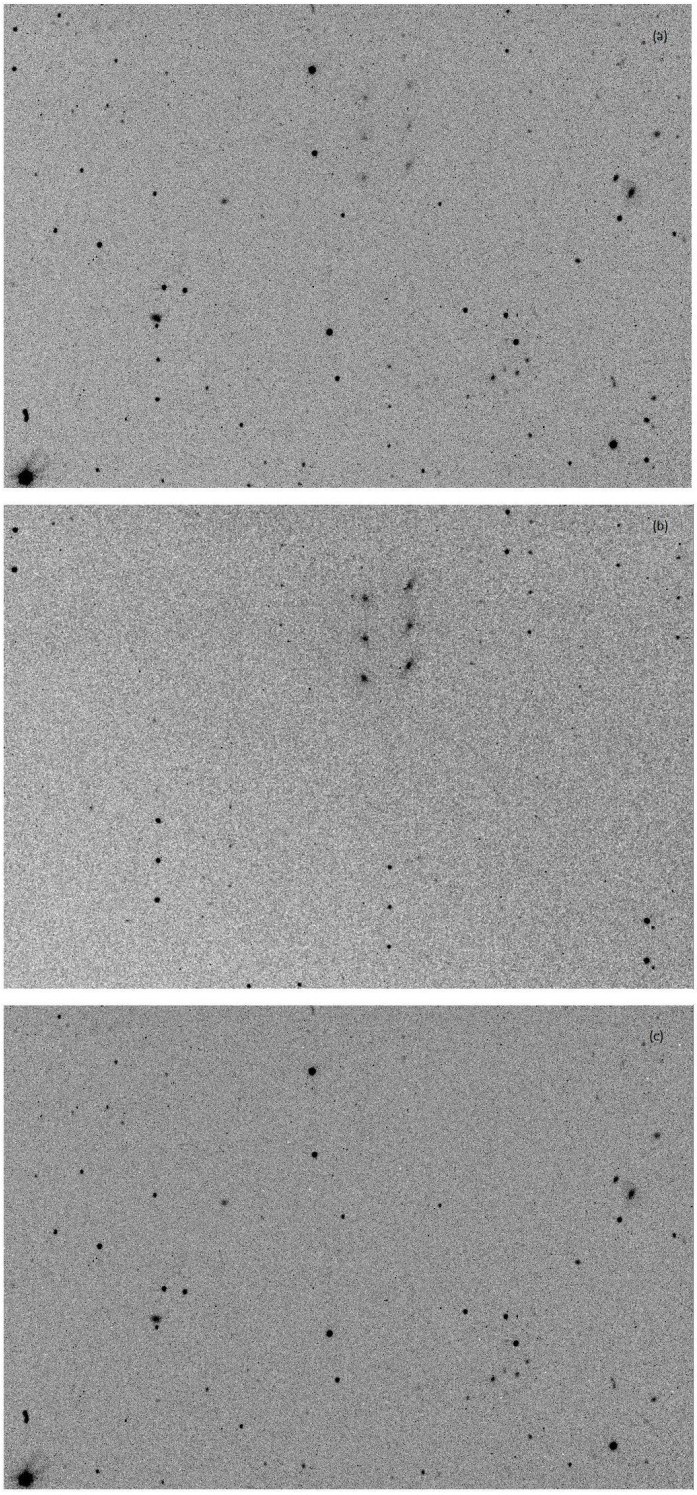

Figure 3: Illustration of RD Afterglow Correction. From top to bottom: (a) image without correction, (b) reduced and median filtered RD, (c) corrected image.

c. Calibration

Table 3 shows dates and some conditions of our Landolt standard star field observations.

Site	Date	Landolt Field	# *	Filter: ExpTime, # of frames	Airmass range
S	2011 July 1	TPHe	6	V: 60s, 3	1.042 - 1.041
S	2011 July 1	PG 1323	5	V: 300s, 2	1.080 - 1.098
N	2011 Apr 28	PG 1323	5	510: 60s-300s, 8	1.334 - 1.349
N	2010 Nov 14	SA 92	6	V: 60s, 2	1.053 - 1.057
N	2011 Apr 28	SA 104	6	V: 30s-90s, 9	1.429 - 1.475
N	2011 Sep 30	SA 113	8	V: 20s-60s, 8	1.209 - 1.248
N	2011 Sep 30	SA 113	7	510: 30s-60s, 6	1.176 - 1.291

Table 3: Observing Information for Landolt Standards. #* is the number of stars in the field observed.

To obtain a relation between count rate and magnitude, we seek the magnitude which gives 1 count per unit exposure time, also called the zero point (ZP). From an image taken in a specified filter (f), we calculate the "raw" magnitude in that filter as m_f= -2.5 log(counts/unit time). In principle standard stars can be used to get the instrumental sensitivity and the atmospheric extinction, k, at each wavelength. Prior research with these telescopes has equipped us with average values of the atmospheric extinction for the most popular filters: mean values for V are k_V=0.17 magnitude/airmass at Kitt Peak and k_V=0.14 magnitude/airmass at Cerro Tololo. We can determine the zero point of a V filter from this equation for corrected V magnitude:

$$V = m_V + ZP_V - k_V X + c_V(B - V) \tag{1}$$

where V, m_V and $k_V$are as mentioned above and X is the airmass, approximately secant (zenith distance). c_V is a transformation term included in the equation to account (to first order) for mismatch in the mean wavelength of our system and the standard one- for V, this term is often negligible and we do not account for it in this calibration. We used IRAF's **imexamine** task to obtain the count rate for a standard star from its radial profile and **hselect** to extract airmass and exposure time from the header.

We use one second for the unit exposure time, and calculate$ZP_{V,N}$= 22.53 ±0.12 for the SARA-N V filter at Kitt Peak and $ZP_{V,S}$= 20.70 ±0.29 for the SARA-S V filter at Cerro Tololo. Dividing the standard deviation$\sigma_{zp}$by the number of zero points N_{zp}gives the zero point error ΔZP. Knowing $ZP_{V,N}$, the mean site extinction k_V, and the gain and read-noise (given in 2.1) let us create surface brightness profiles with IRAF's**phot** task in the digiphot.appphot package.

To convert to flux per Å within the filter, we follow [8] and calculate

F_0= 3.6e-9 erg/(cm^{2}sÅ)*$10^{-ZP/(2.5)}$:

$$F_{0,V(N)} = 3.518(^{+0.36}/_{-0.39}) \cdot 10^{-18}\, erg\, cm^{-2} s^{-1} \mathring{A}^{-1} \tag{2}$$

$$F_{0,f510} = R \cdot F_{0,N} = 1.971(^{+0.31}/_{-0.34}) \cdot 10^{-17}\, erg\, cm^{-2} s^{-1} \mathring{A}^{-1} \tag{3}$$

$$F_{0,L} = R \cdot EW_{f510} \cdot F_{0,f510} \approx 1.7 \cdot 10^{-15}\, erg\, cm^{-2} s^{-1} \tag{4}$$

R in Equation 3 is the ratio of counts per unit time of a star in V / counts per unit time of the star in f510. The SA113 field observations with SARA-N give an average value of R = 5.6±0.3. The effective width (EW) in Equation 4 is about 85 Å for our f510 filter. Testing the fluxes for the well-studied NGC 6240 lets us check our calibration: (check/compare). Lastly, since the emission line will come in to f510 off-center for redshifts near the edges of our range, we multiply $F_{0,L}$ by a correction factor p(z) in those cases. f10's peak transmission has a value 0.81 and let the peak transmission value of λ5007 for a given z be called T_z:

$$p_z = \frac{0.81}{T_z} \tag{5}$$

$$F_{0*,L} \approx p_z \cdot 1.7 \cdot 10^{-15}\, erg\, cm^{-2} s^{-1} \tag{6}$$

4. IMAGES

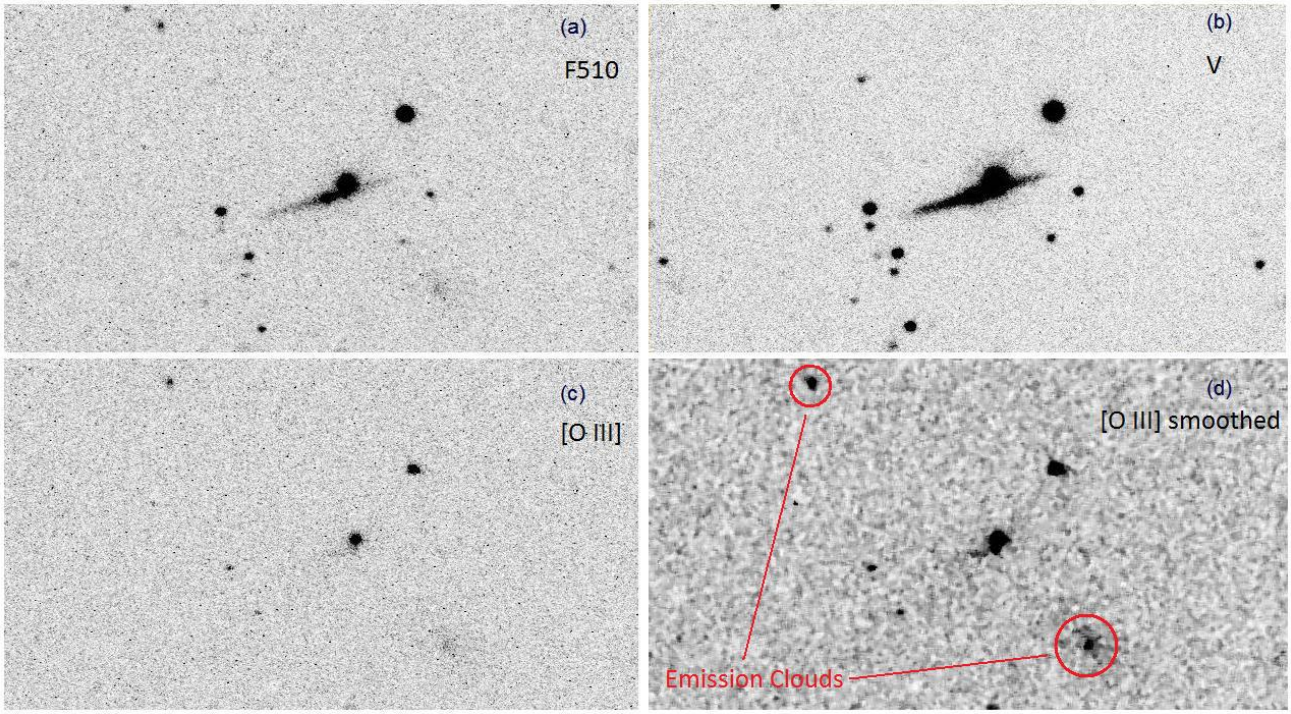

Figure 4: Example of an image set (inverted color)

Figure 4 shows an example of an image set for a galaxy. In this section in Figures 5-43, we present the combined f510 & V images, e.g. Figure 4(a) and 4(b), overlayed with contours from the smoothed emission line image, e.g. Figure 4(d). In all figures, North is at the top and East is to the left. Observational parameters for these images are listed in Table 4. The galaxy is circled in cyan if it is not obvious or the field is crowded.

MARK 341 / NGC 0169A

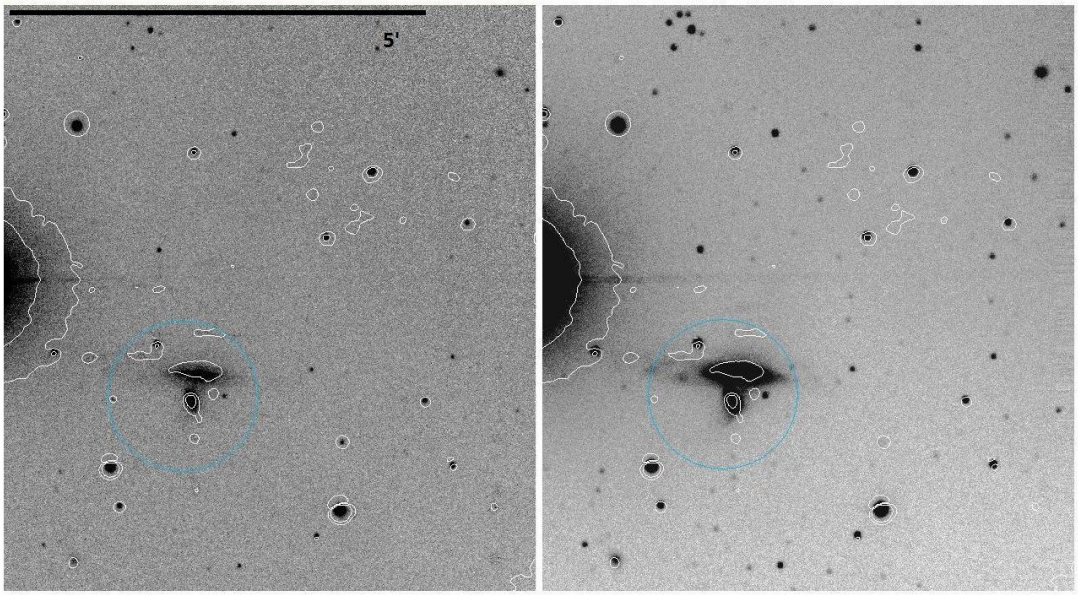

Figure 5: MARK 341. F510 & V images overlayed with smoothed [O III]-line image contours.

Mrk 352

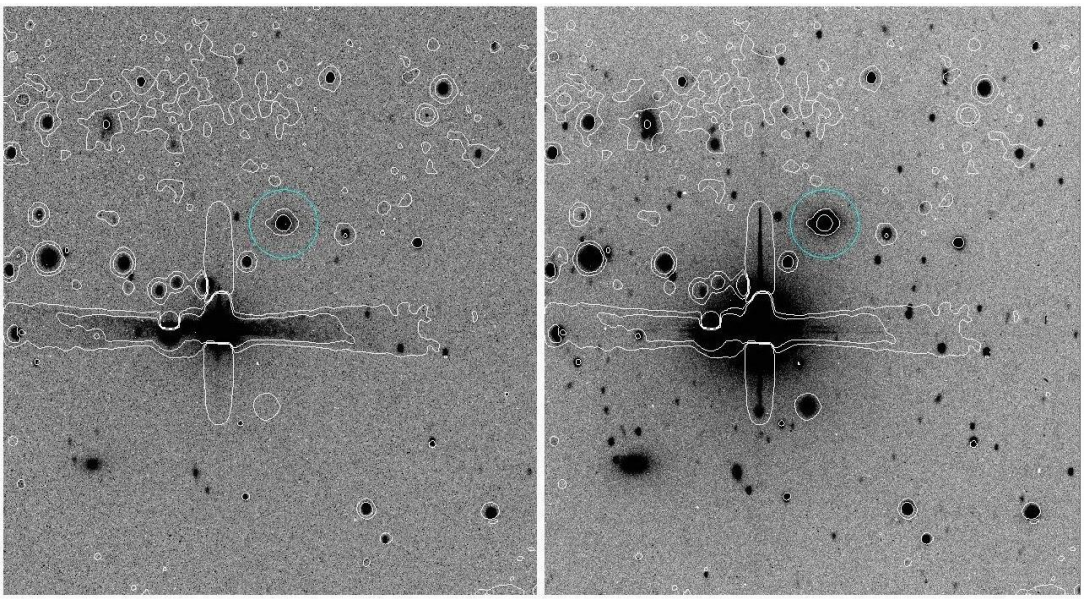

Figure 6: Mrk 352. F510 & V images overlayed with smoothed [O III]-line image contours.

Mrk 1 / NGC 0449

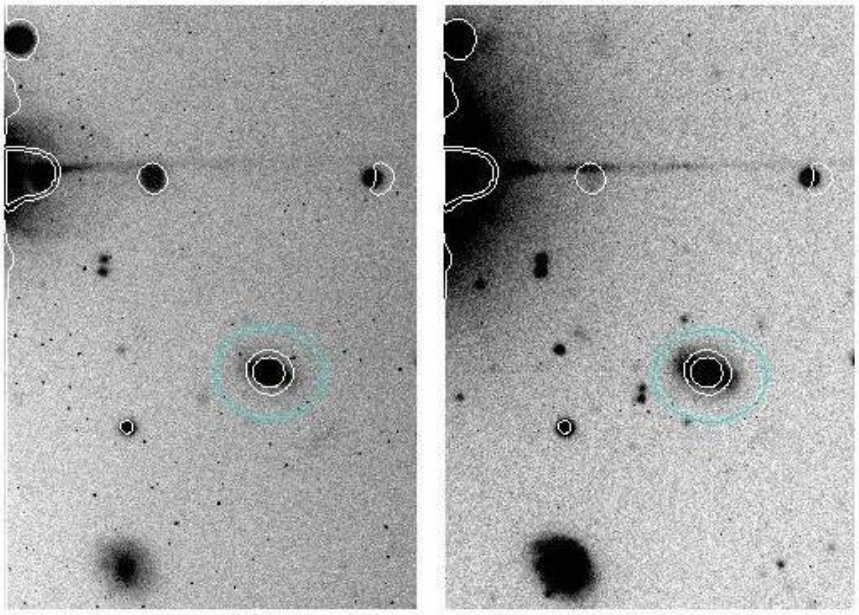

Figure 7: Mrk 1. F510 & V images overlayed with smoothed [O III]-line image contours. The [O III] feature to the NE of Mrk 1 is due to an afterglow effect.

NGC 0513

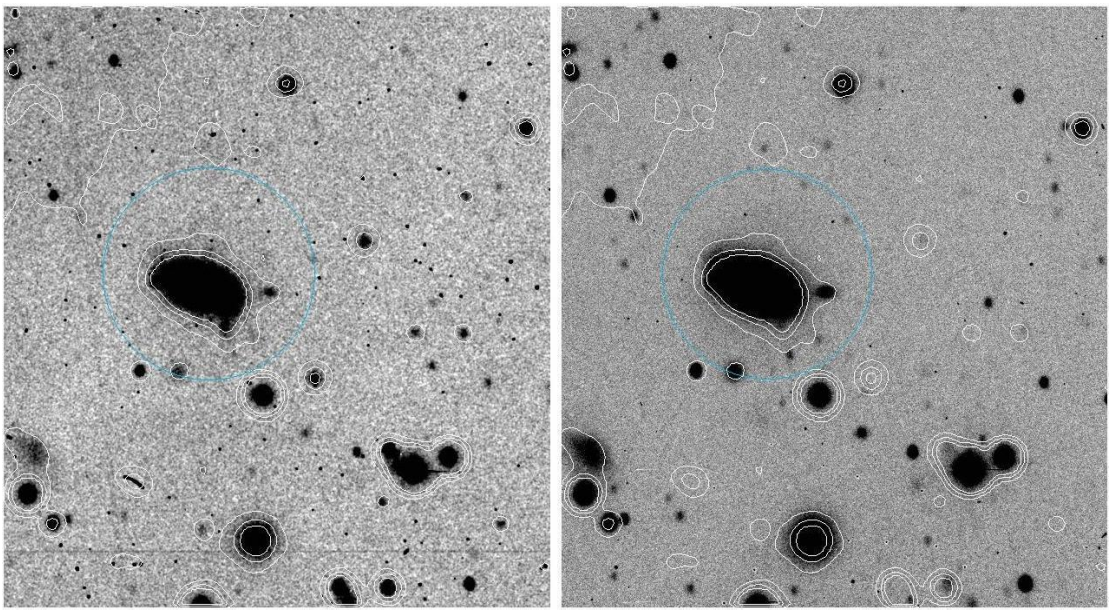

Figure 8: NGC 513. F510 & V images overlayed with smoothed [O III]-line image contours.

Mrk 993 / UGC 00987

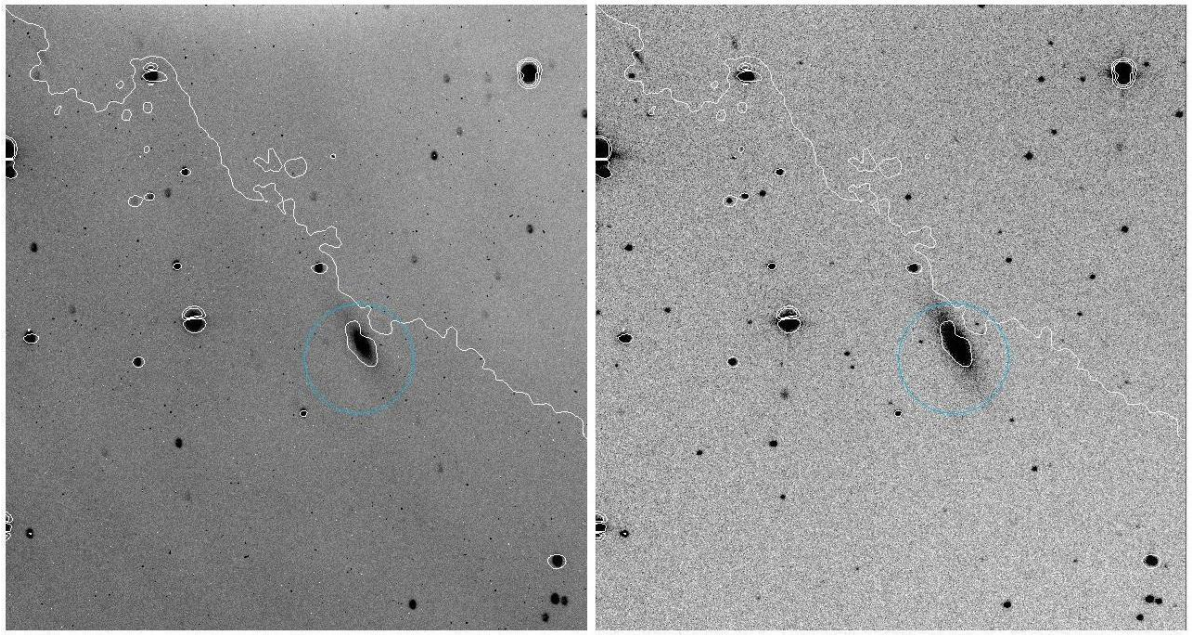

Figure 9: Mrk 993. F510 & V images overlayed with smoothed [O III]-line image contours.

Mrk 359 / UGC 01032

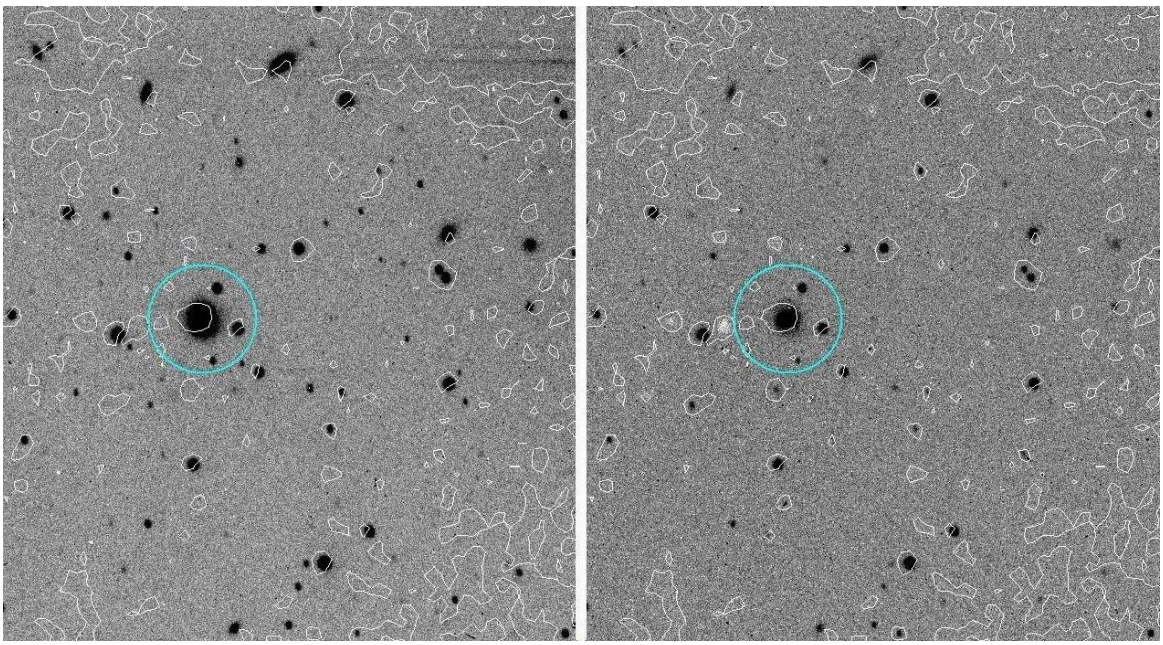

Figure 10: Mrk 359. F510 & V images overlayed with smoothed [O III]-line image contours.

UGC 01395

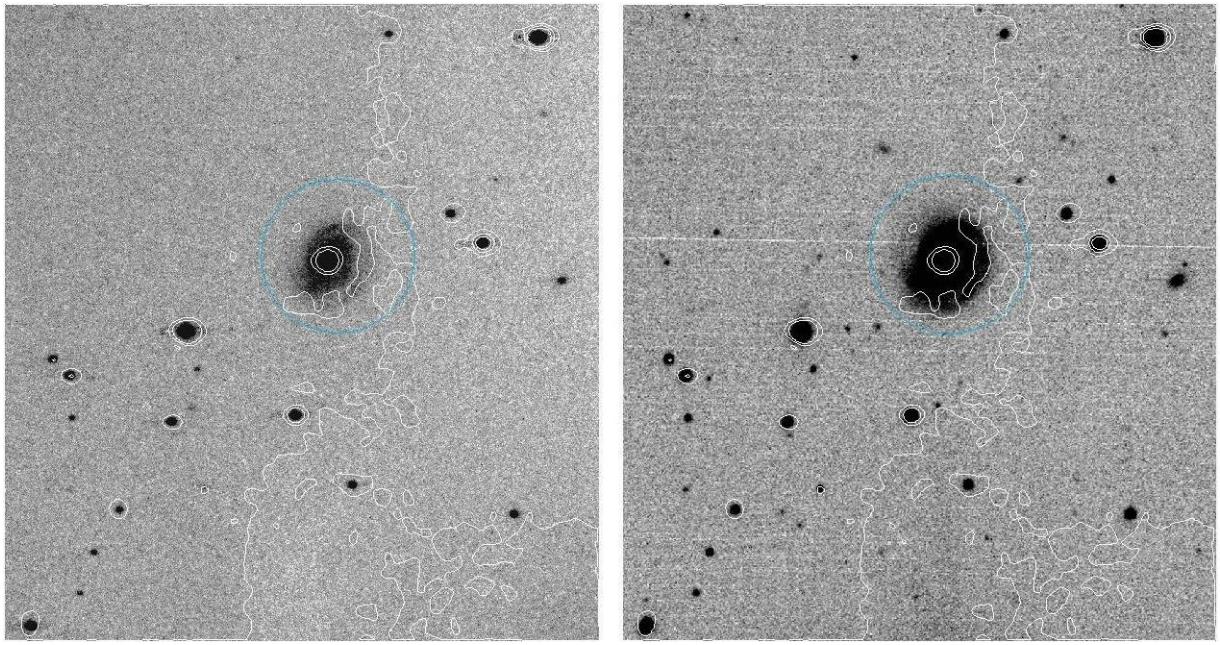

Figure 11: UCG 1395. F510 & V images overlayed with smoothed [O III]-line image contours.

NGC 0841

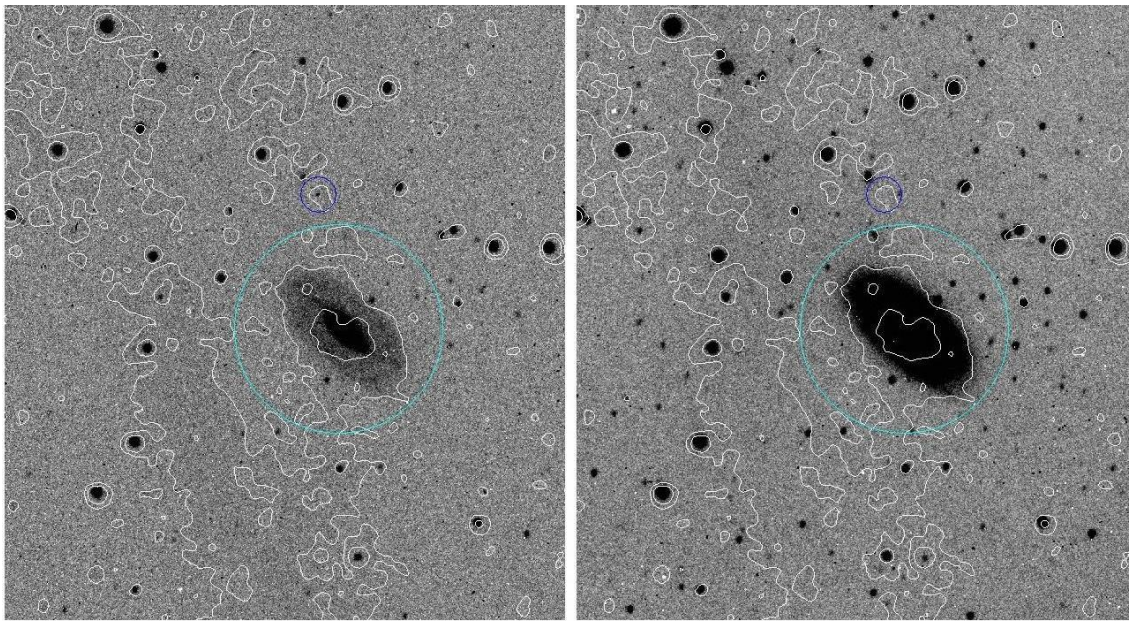

Figure 12: NGC 841. F510 & V images overlayed with smoothed [O III]-line image contours. One [O III] structure. not correlated with HI map. likely an EL dot.

Mrk 1040

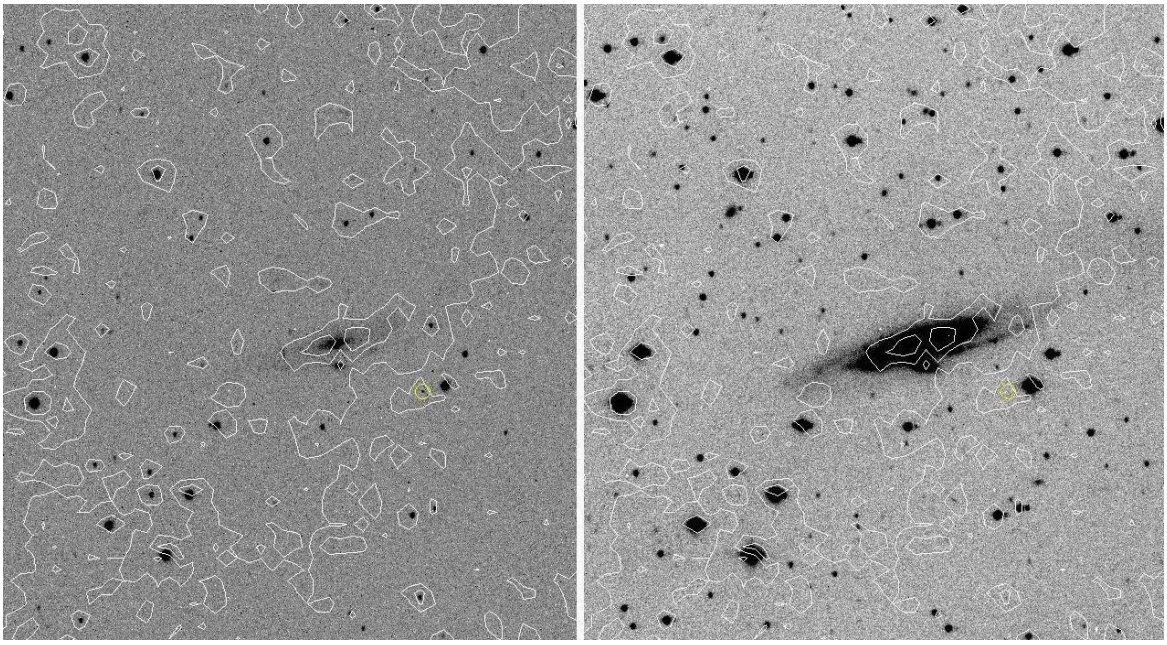

Figure 13: Mrk 1040. F510 & V images overlayed with smoothed [O III]-line image contours.

NGC 0973

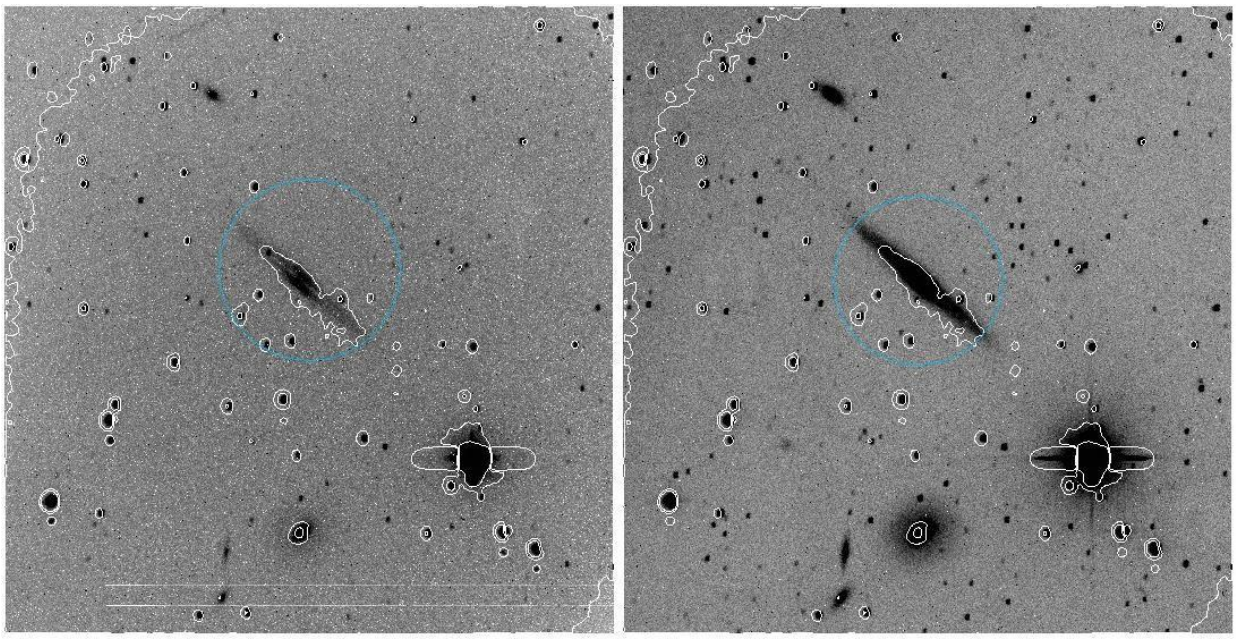

Figure 14: NGC 973. F510 & V images overlayed with smoothed [O III]-line image contours.

NGC 1167

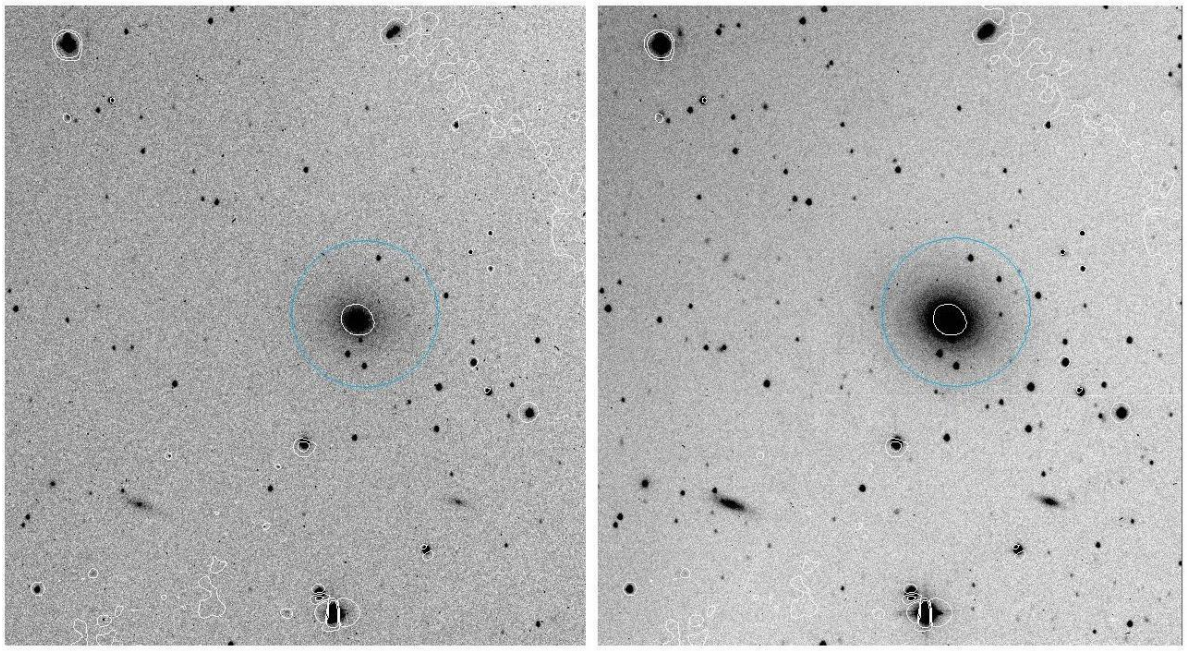

Figure 15: NGC 1167. F510 & V images overlayed with smoothed [O III]-line image contours.

UGC 03157

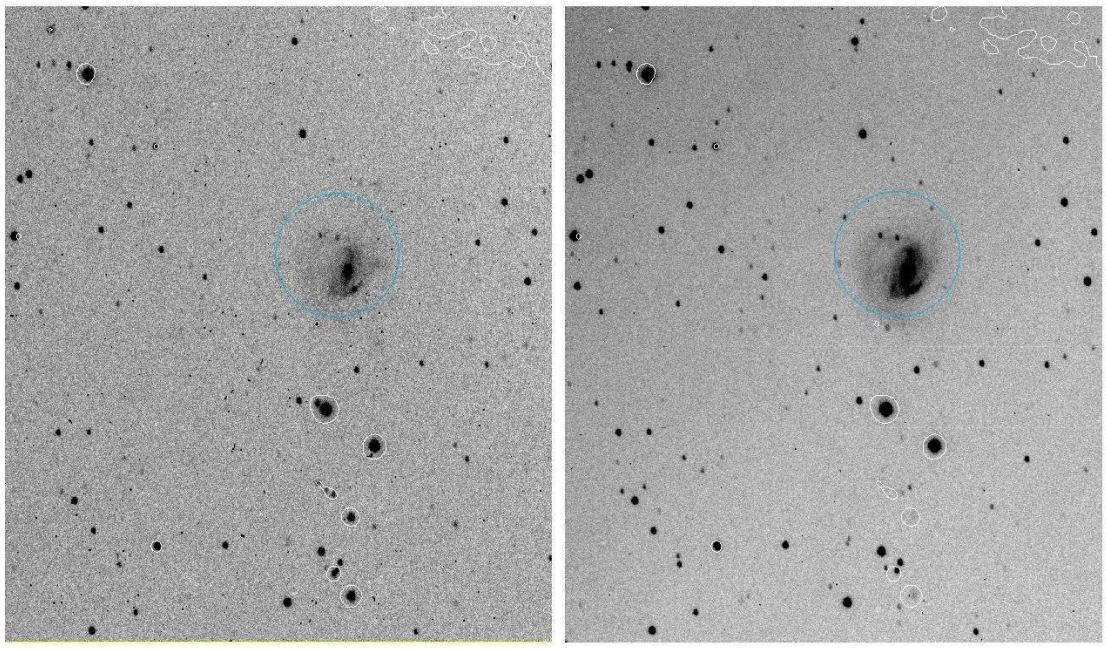

Figure 16: UGC 3157. F510 & V images overlayed with smoothed [O III]-line image contours.

MS 04595+0327 / 2MASX J0520903+0331499

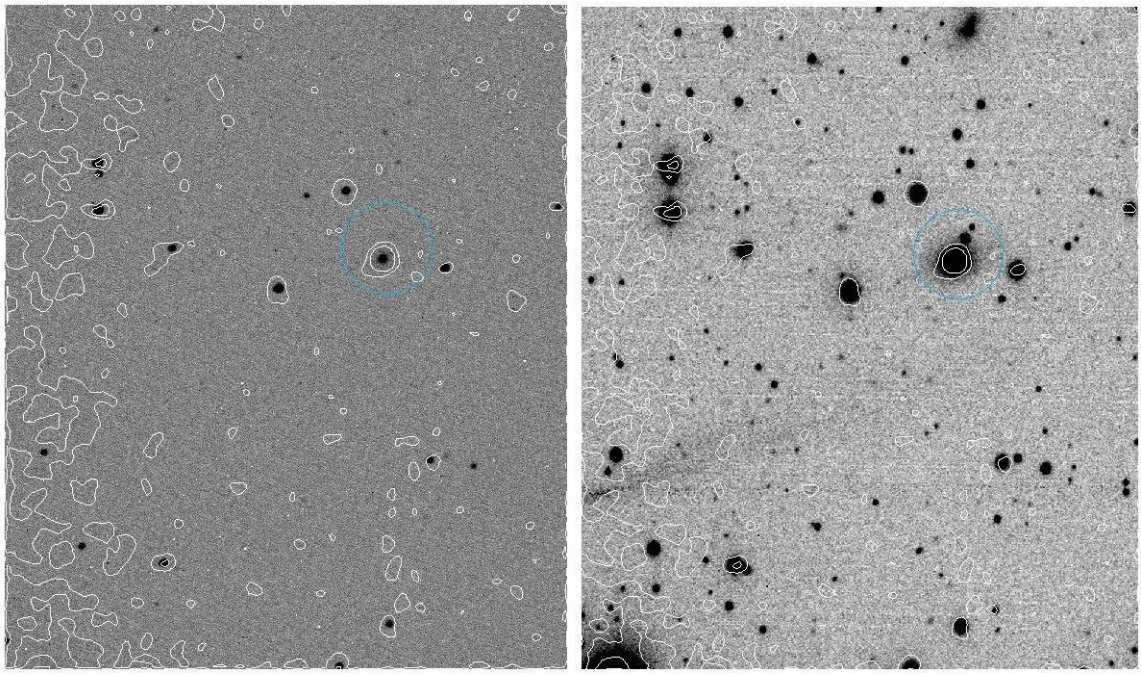

Figure 17: MS 04595+0327. F510 & V images overlayed with smoothed [O III]-line image contours.

2E 0507+1626 / IRAS 05078+1626

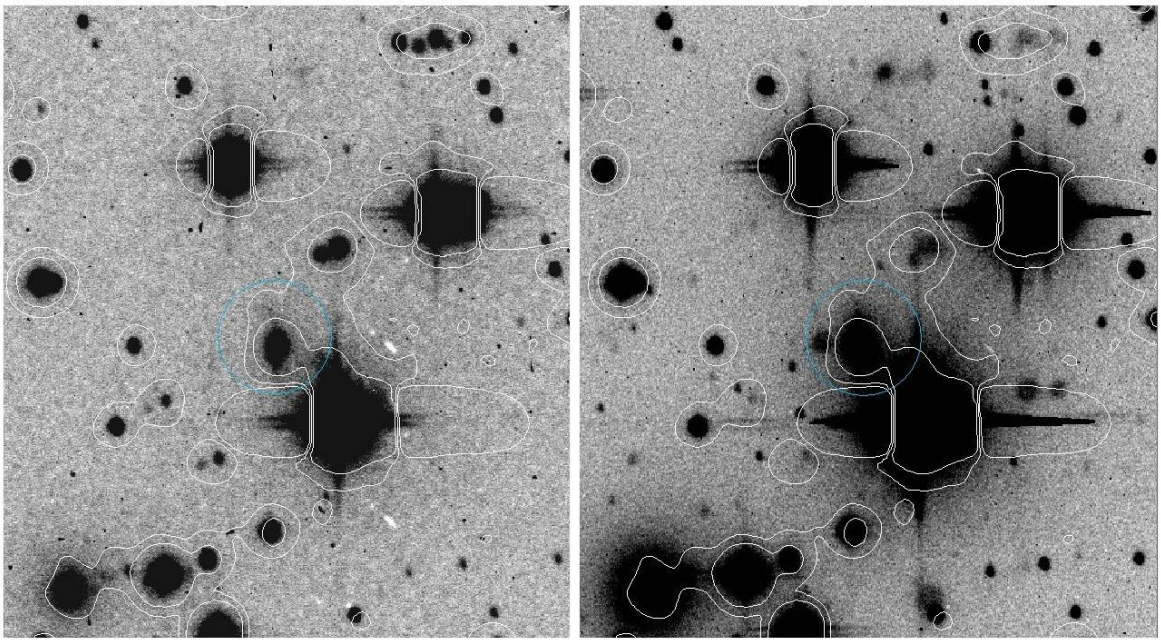

Figure 18: 2E 0507+1626. F510 & V images overlayed with smoothed [O III]-line image contours.

MCG -04.16.001 / ESO 489- G 047

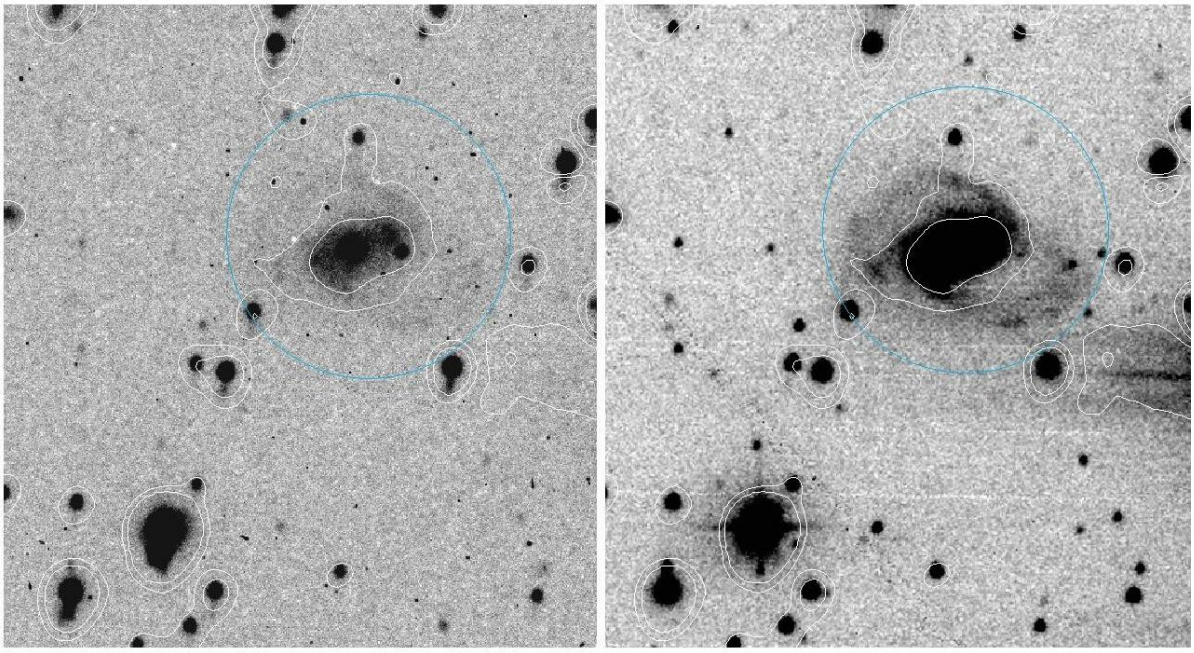

Figure 19: MCG -04.16.001. F510 & V images overlayed with smoothed [O III]-line image contours.

UGC 03478

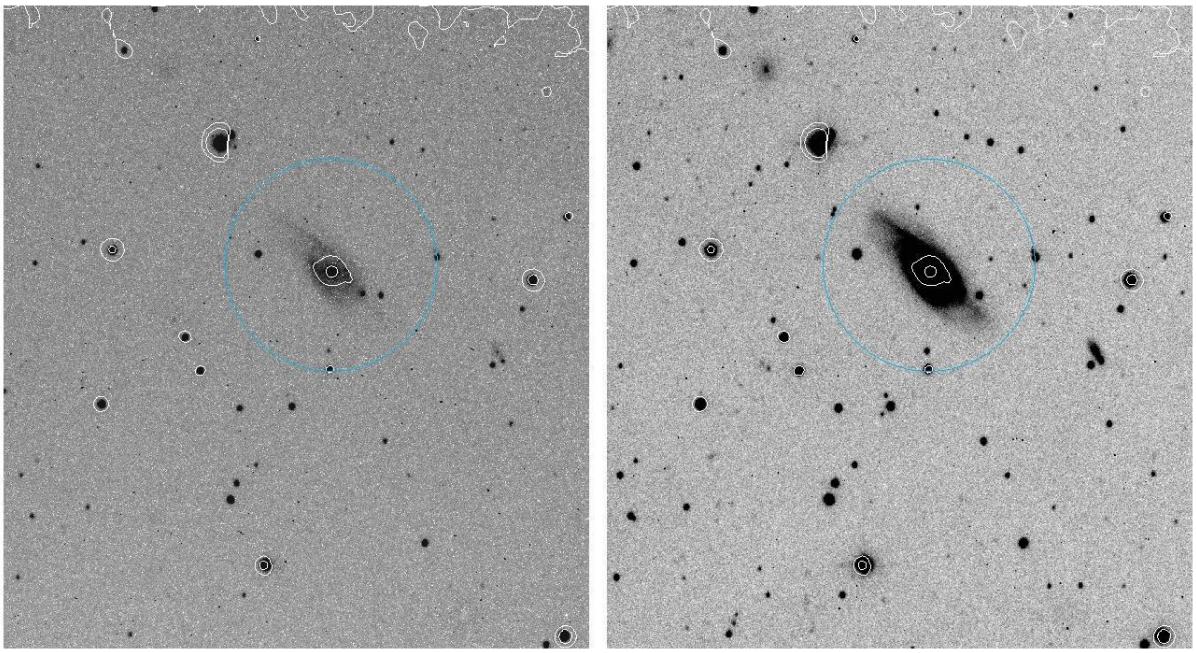

Figure 20: UGC 03478. F510 & V images overlayed with smoothed [O III]-line image contours.

UGC 03995

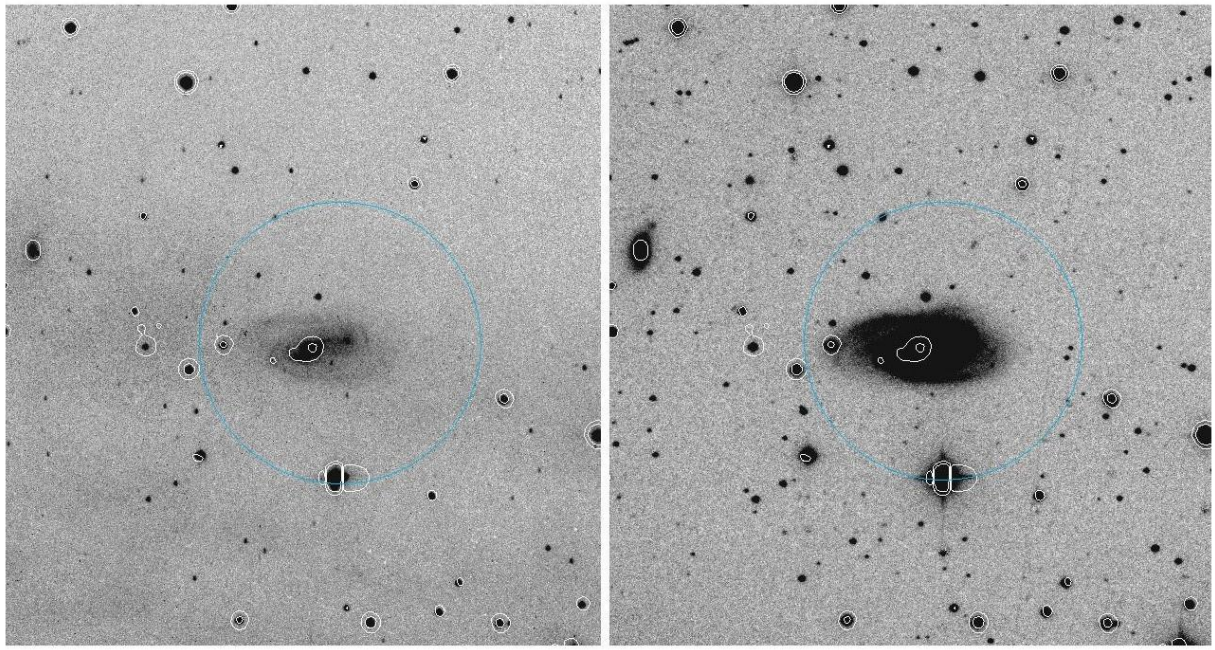

Figure 21: UGC 03995. F510 & V images overlayed with smoothed [O III]-line image contours.

NGC 2639

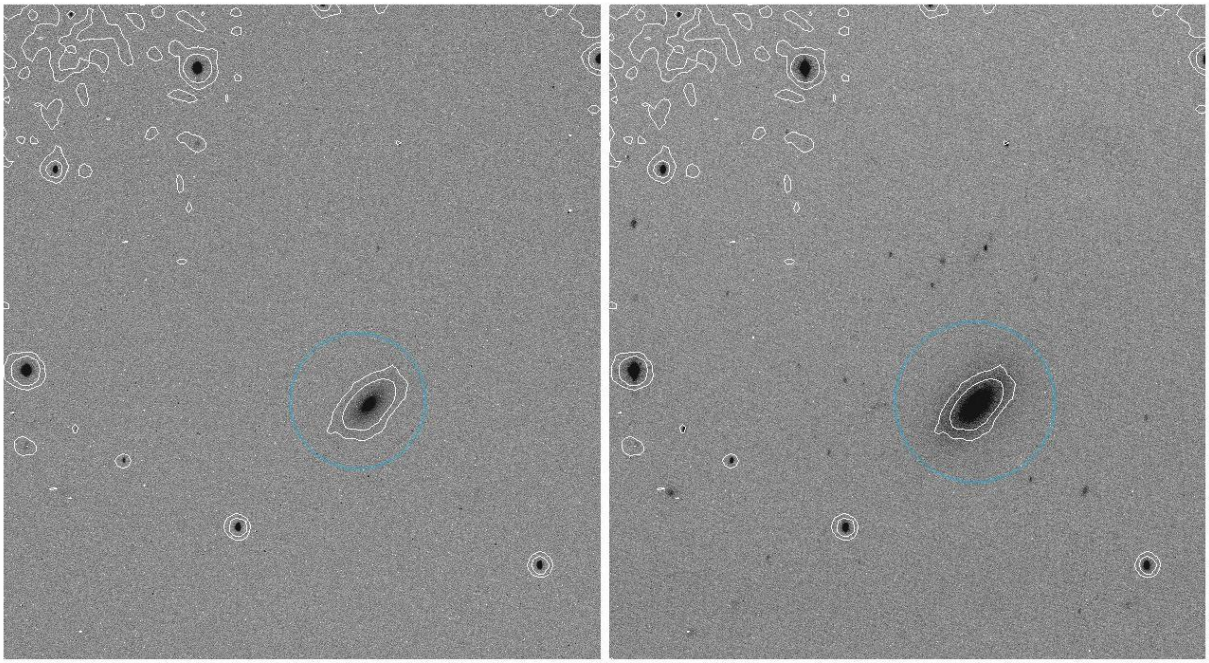

Figure 22: NGC 2639. F510 & V images overlayed with smoothed [O III]-line image contours.

NGC 2824

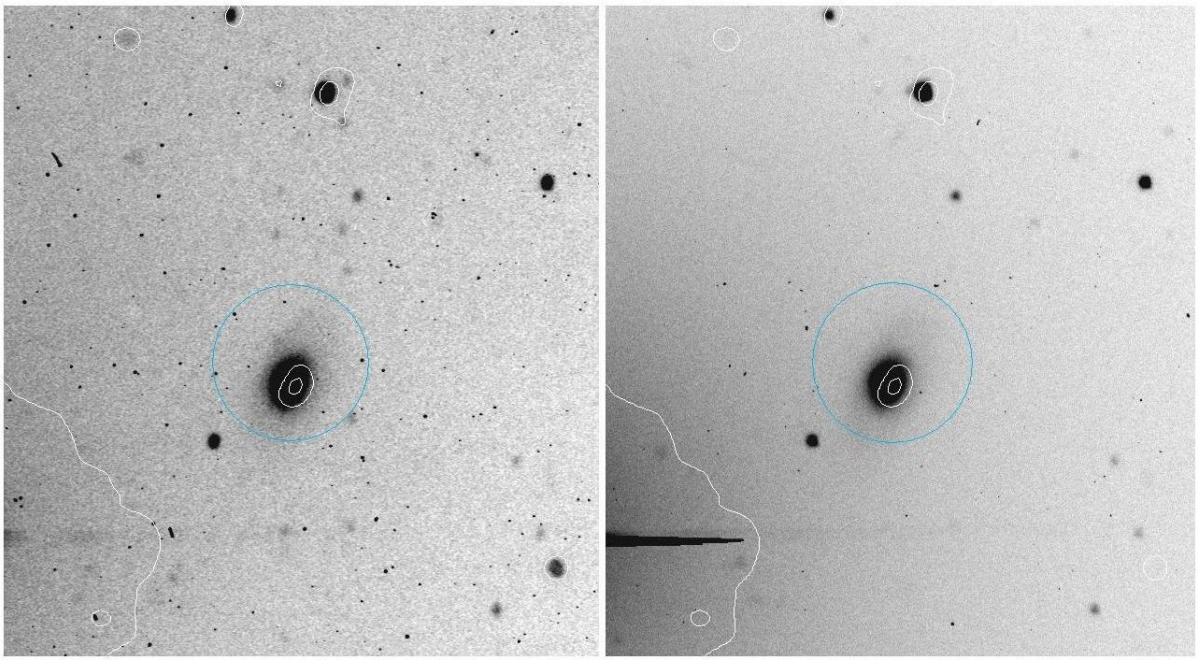

Figure 23: NGC 2824. F510 & V images overlayed with smoothed [O III]-line image contours.

MCG -01.24.012

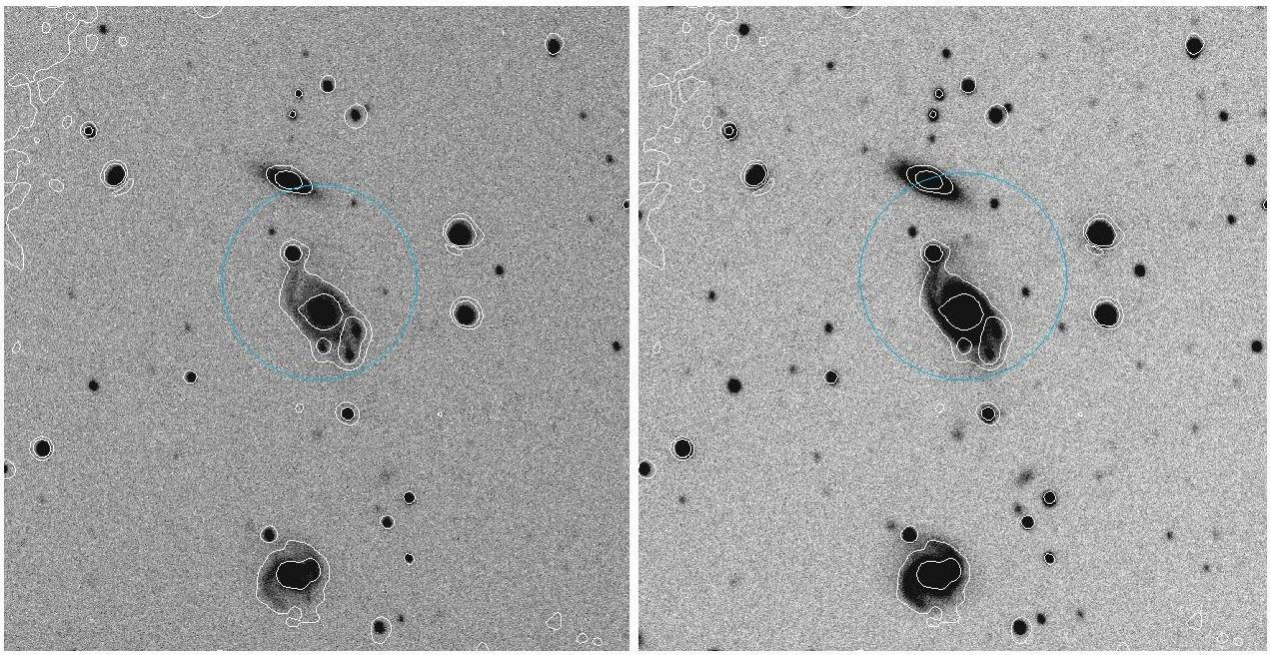

Figure 24: MCG -01.24.012. F510 & V images overlayed with smoothed [O III]-line image contours.

Mrk 1419 / NGC 2960

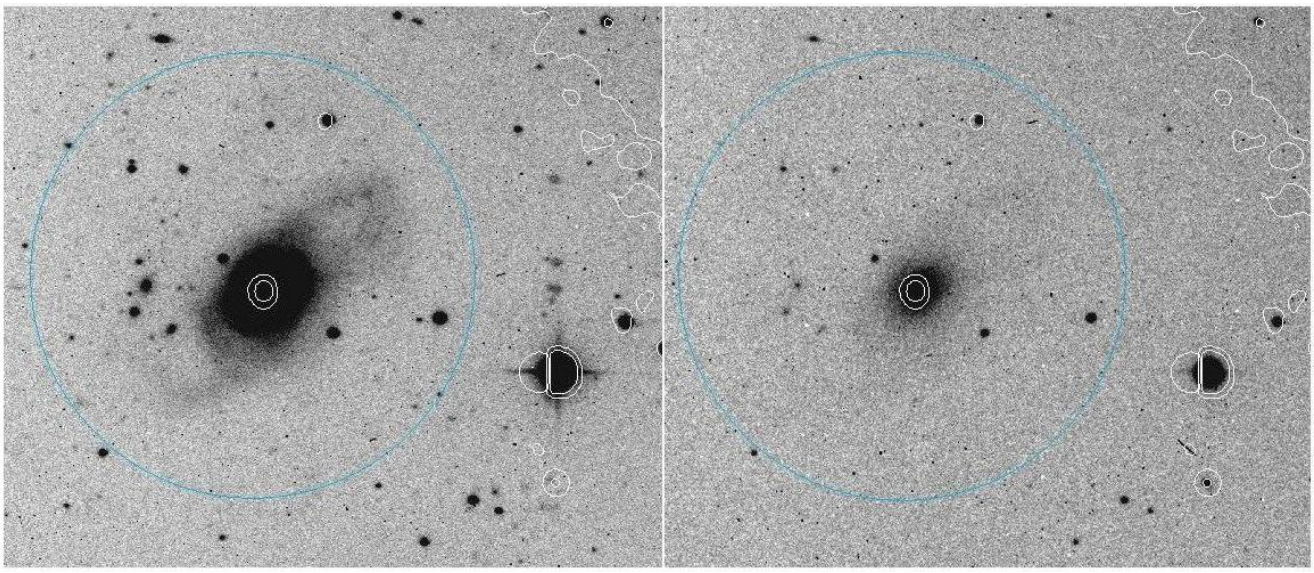

Figure 25: Mrk 1419. F510 & V images overlayed with smoothed [O III]-line image contours.

RXS J11032-0654 / LCRS B110045.0-063806

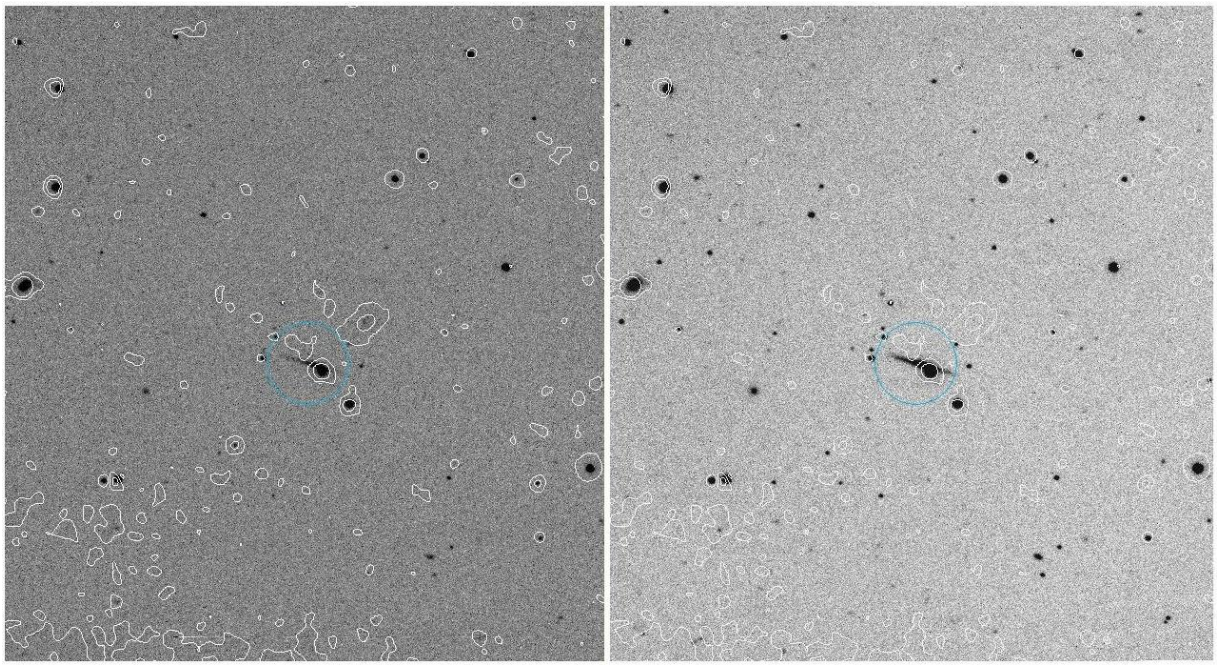

Figure 26: RXS J11032-0654. F510 & V images overlayed with smoothed [O III]-line image contours. This is the S1 with extended emission-line clouds found by this study.

NGC 3822

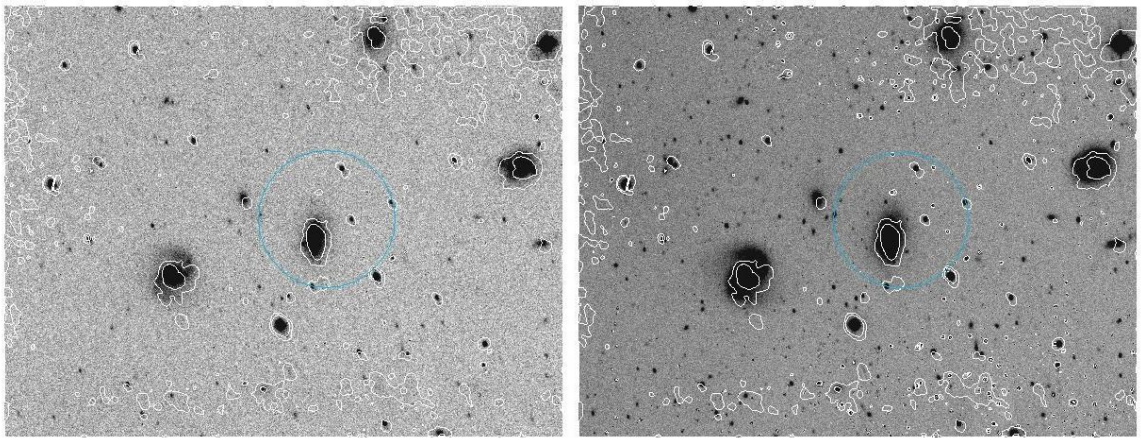

Figure 27: NGC 3822. F510 & V images overlayed with smoothed [O III]-line image contours.

NGC 4404

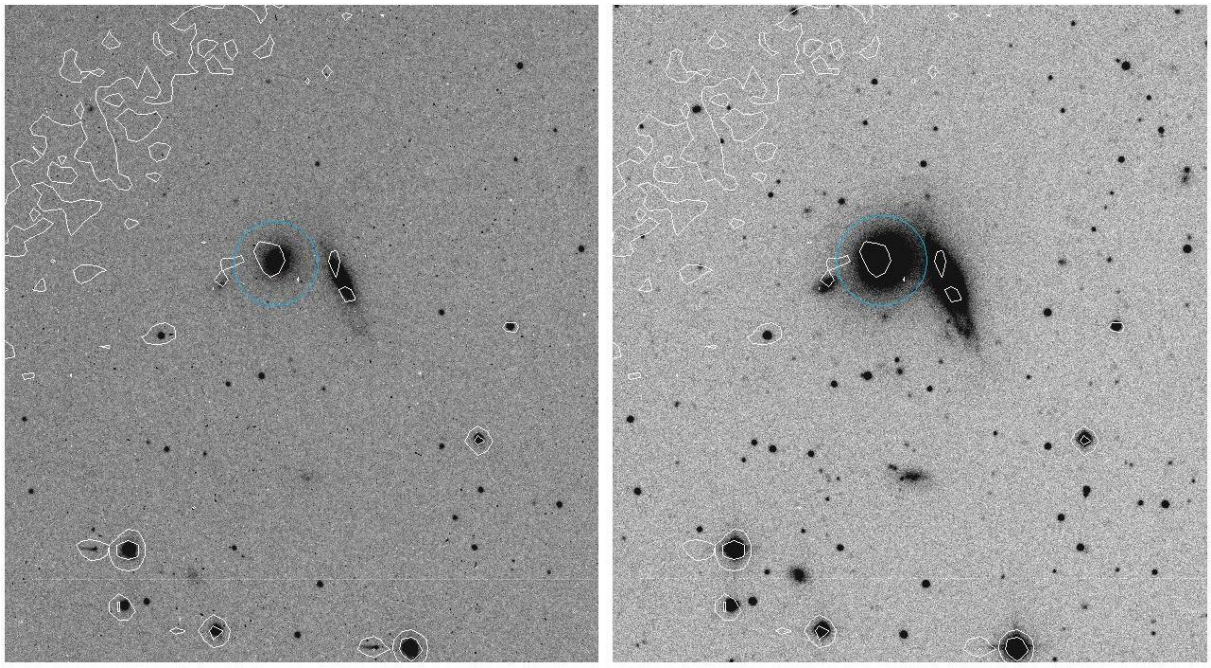

Figure 28: NGC 4404. F510 & V images overlayed with smoothed [O III]-line image contours.

NGC 4619

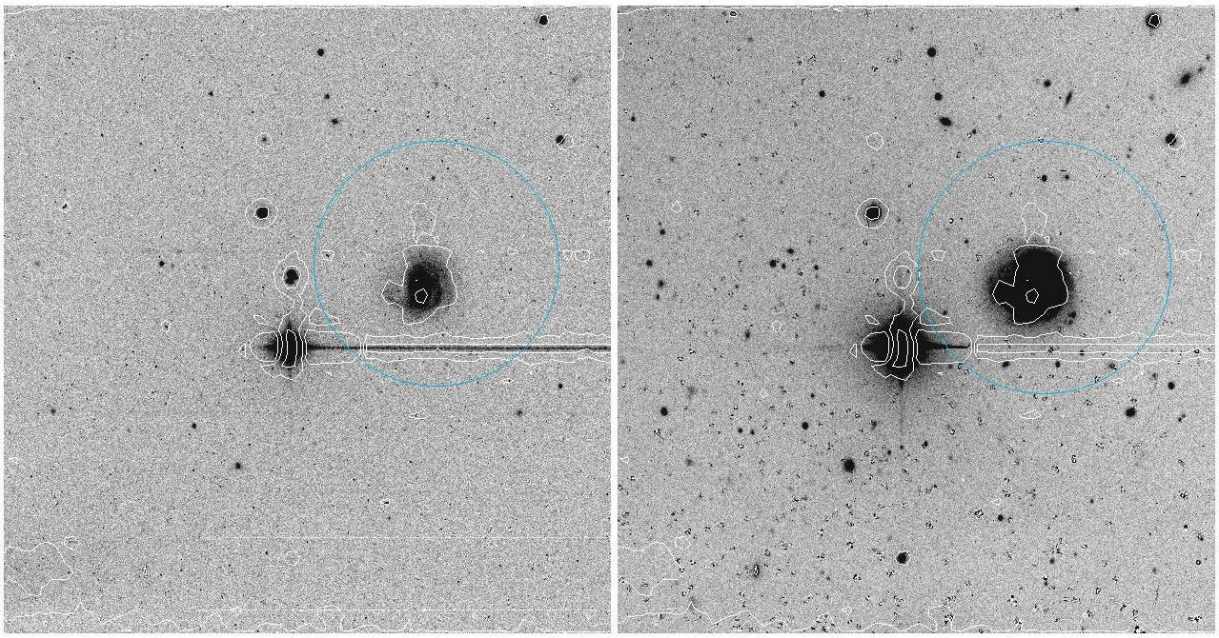

Figure 29: NGC 4619. F510 & V images overlayed with smoothed [O III]-line image contours.

3C 278 / V V ***201***

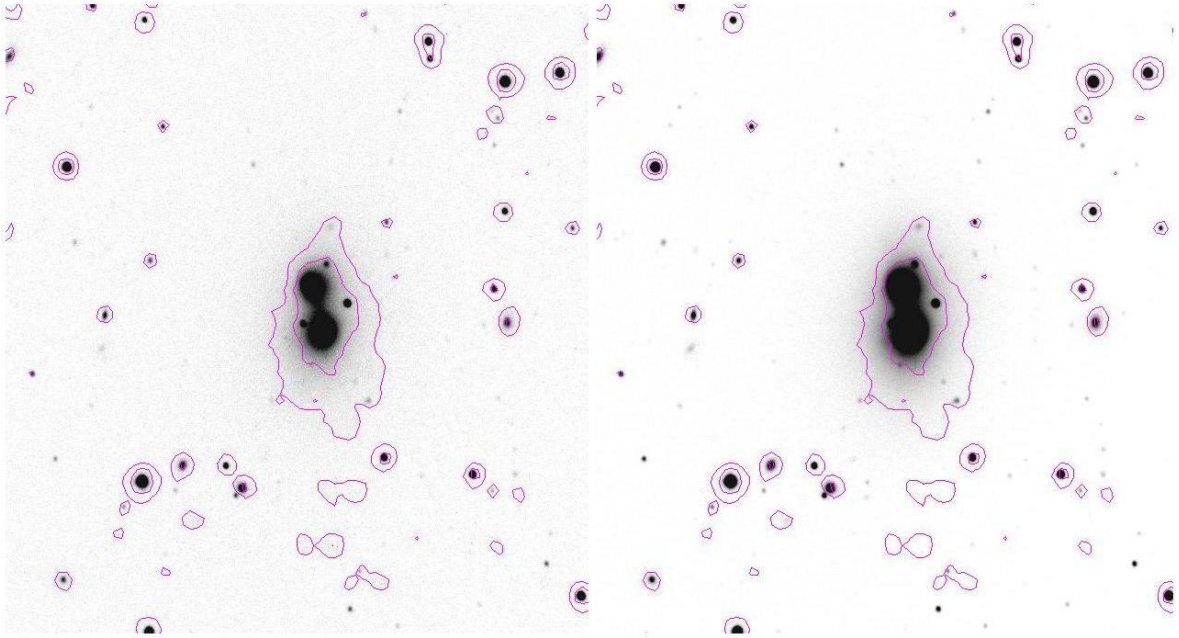

Figure 30: 3C 278. F510 & V images overlayed with smoothed [O III]-line image contours. (Note: logarithmic instead of linear scaling was used for the display.)

Mrk 461 / UGC 08718

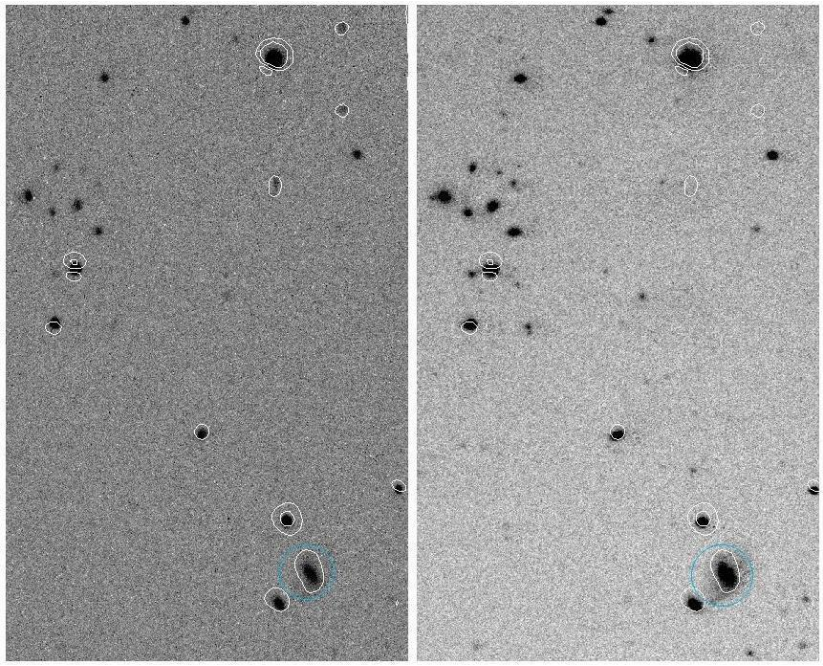

Figure 31: Mrk 461. F510 & V images overlayed with smoothed [O III]-line image contours.

IRAS 14082+1347 / CGCG 074-129

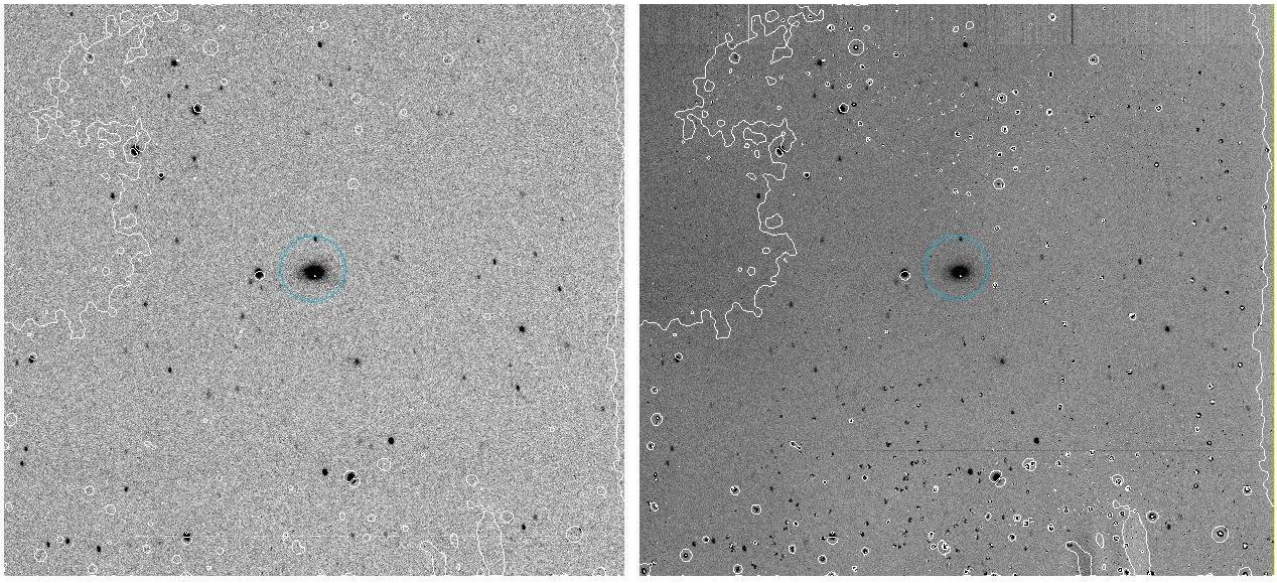

Figure 32: IRAS 14082+1347. F510 & V images overlayed with smoothed [O III]-line image contours.

Mrk 1510 / IC 4397

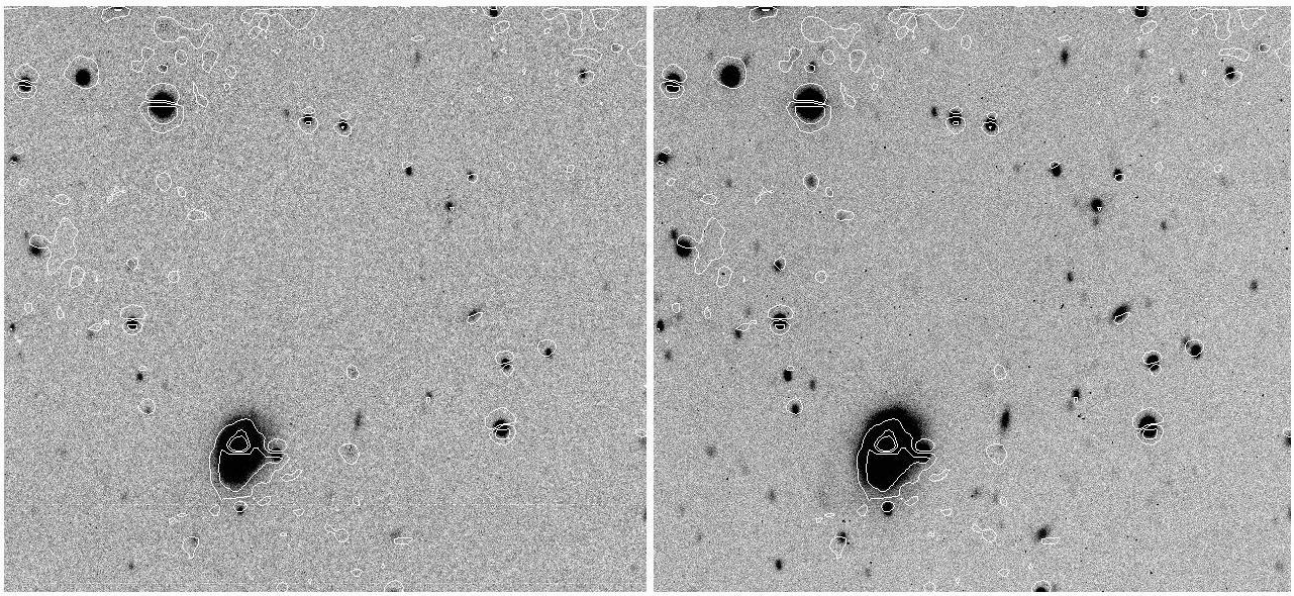

Figure 33: Mrk 1510. F510 & V images overlayed with smoothed [O III]-line image contours.

NGC 5548

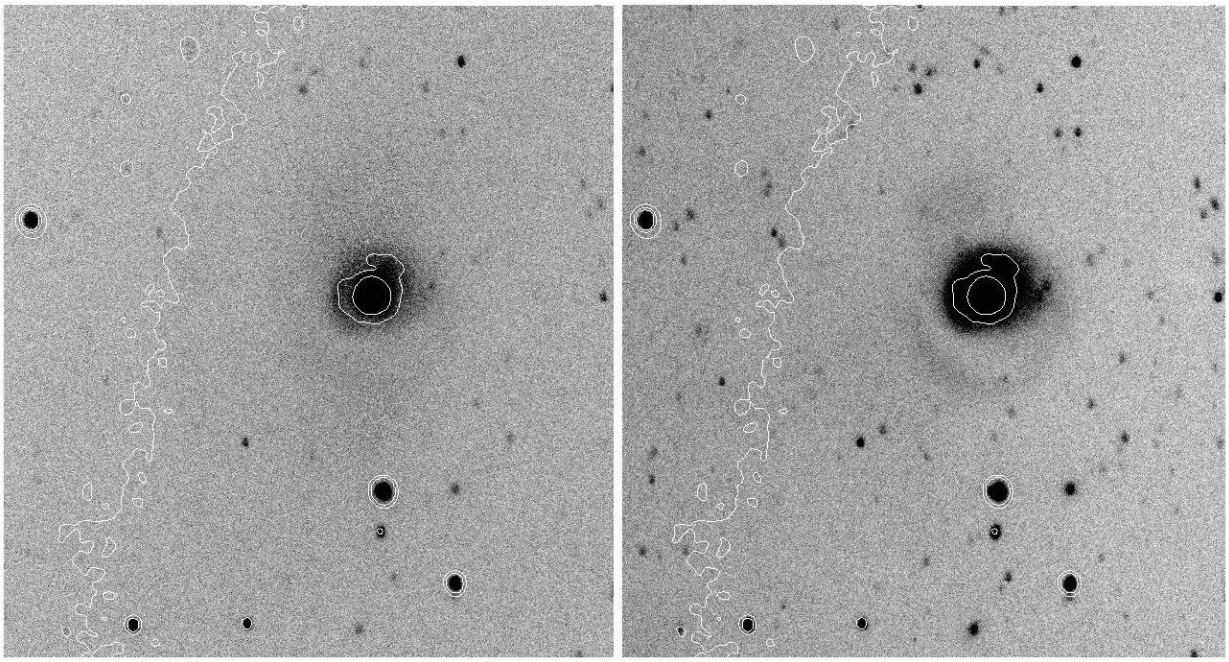

Figure 34: NGC 5548. F510 & V images overlayed with smoothed [O III]-line image contours.

Zw 338.014 / CGCG 338-014

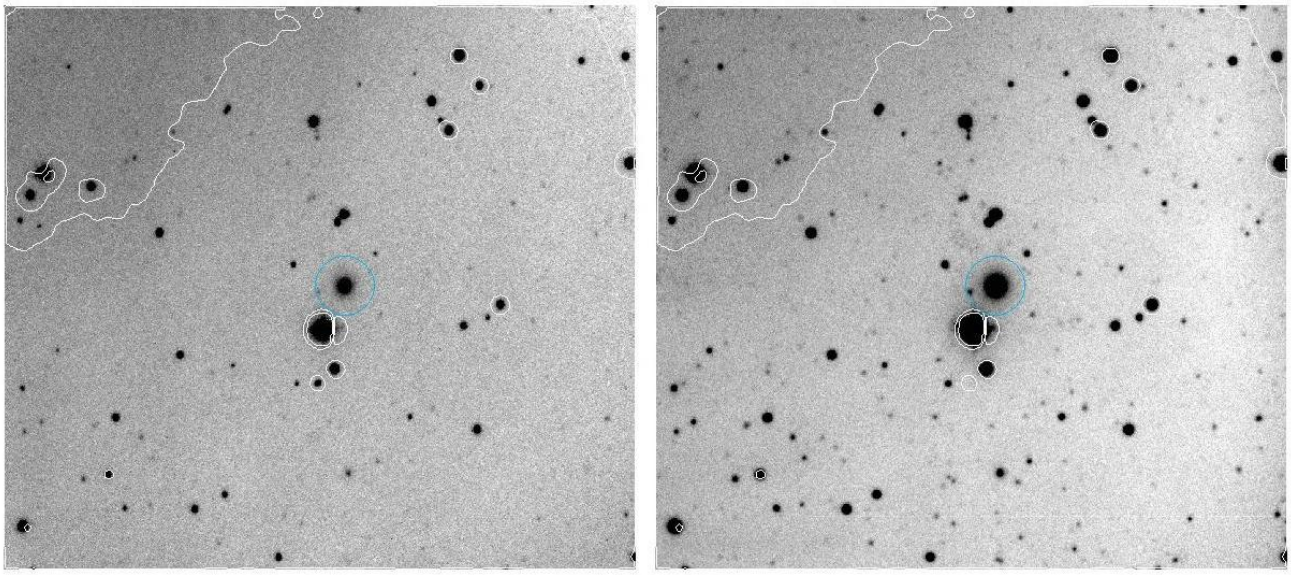

Figure 35: Zw 338.014. F510 & V images overlayed with smoothed [O III]-line image contours.

NGC 6240

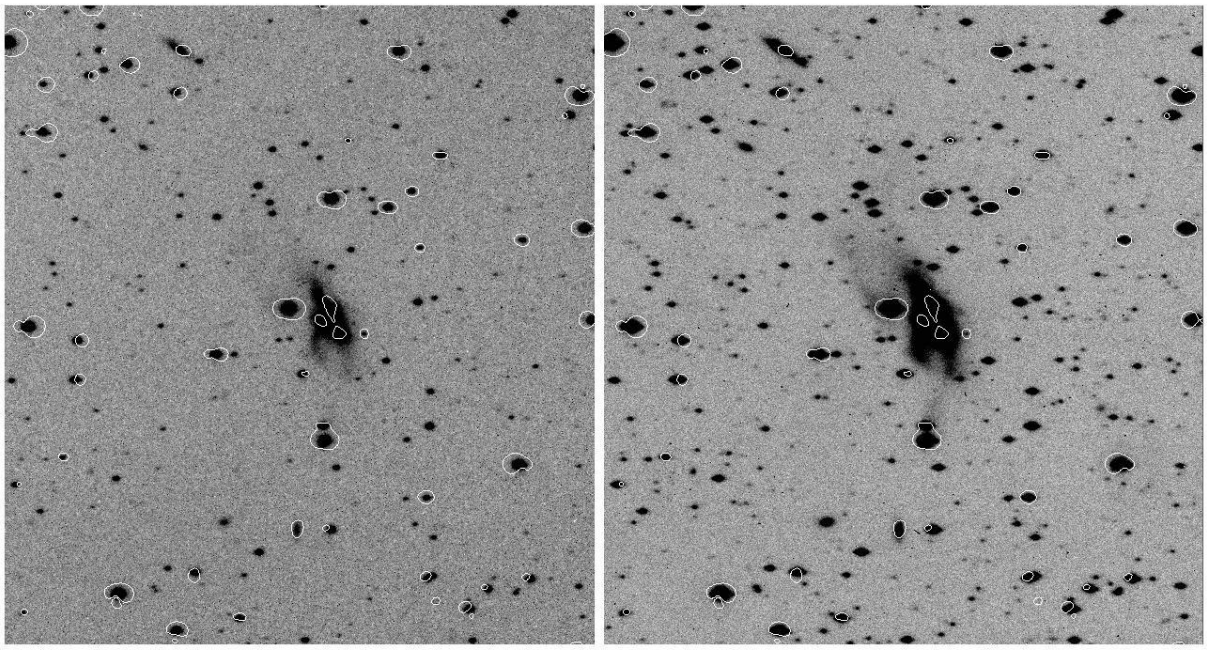

Figure 36: NGC 6240. F510 & V images overlayed with smoothed [O III]-line image contours.

Ark 539

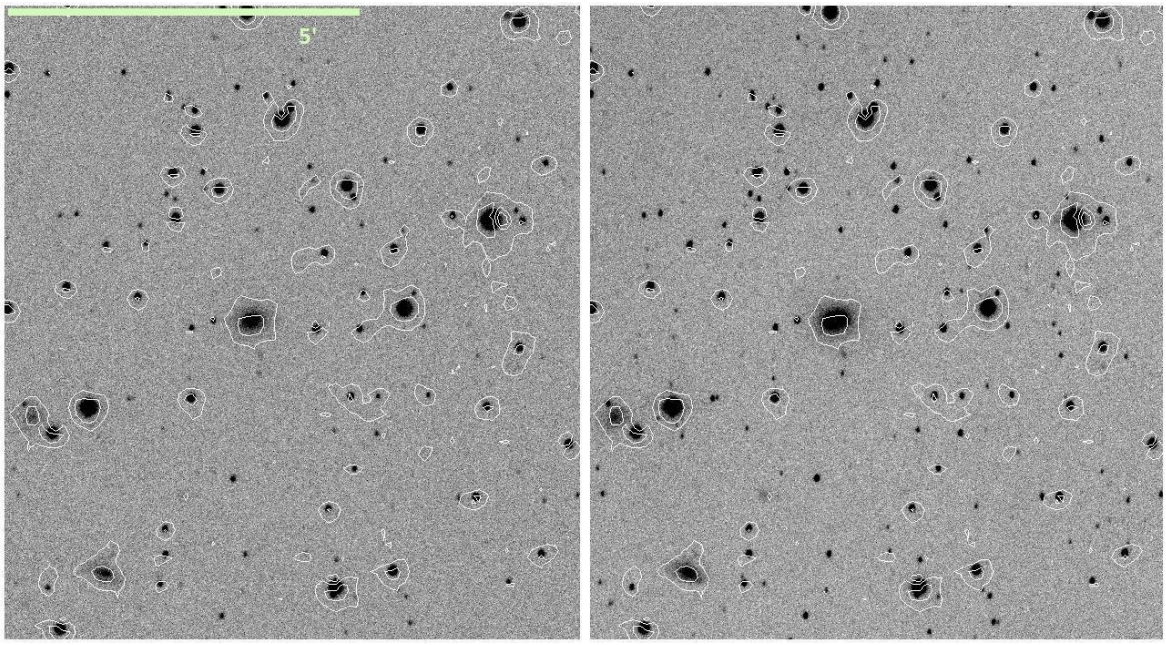

Figure 37: Ark 539. F510 & V images overlayed with smoothed [O III]-line image contours.

UGC 11630 / NGC 6967

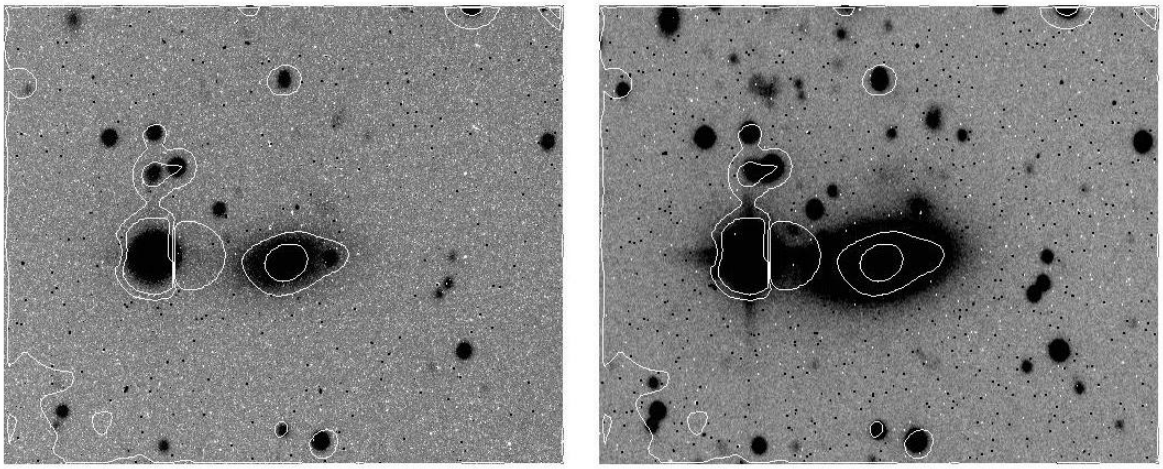

Figure 38: UGC 11630. F510 & V images overlayed with smoothed [O III]-line image contours.

NGC 7469

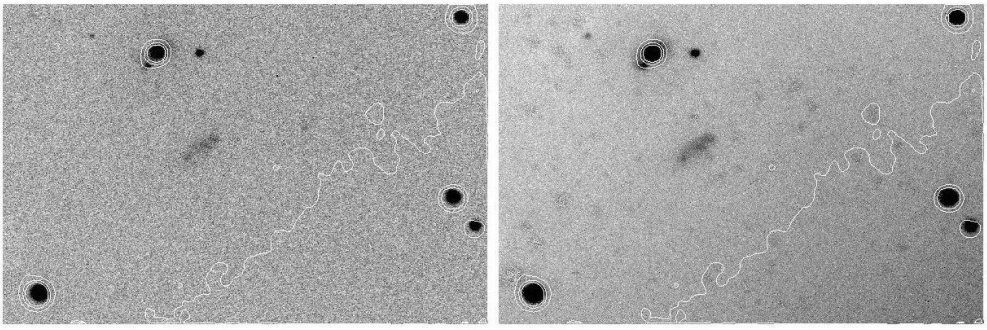

Figure 39: NGC 7469. F510 & V images overlayed with smoothed [O III]-line image contours.

IC 1515

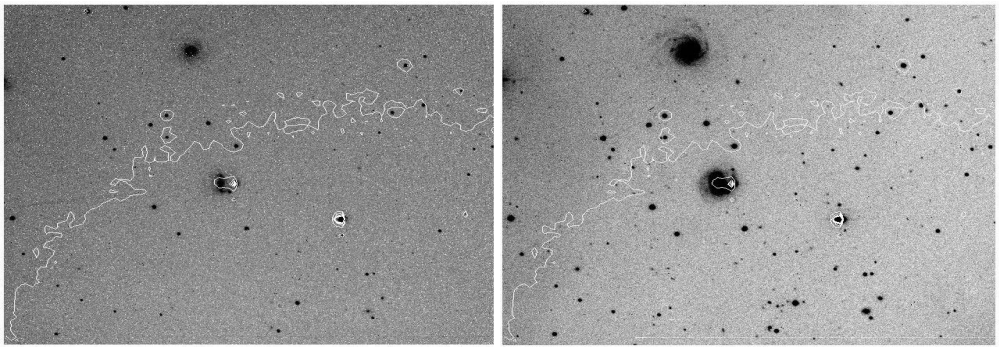

Figure 40: IC 1515. F510 & V images overlayed with smoothed [O III]-line image contours.

ESO 602- G 025

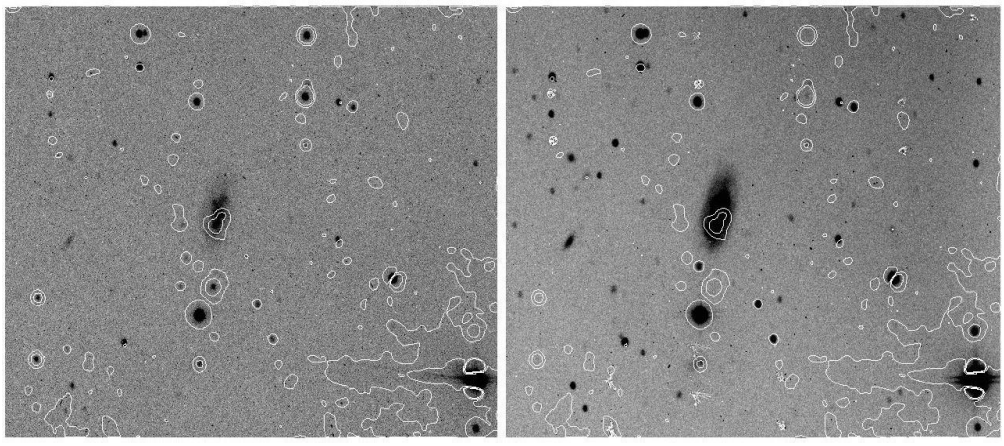

Figure 41: ESO 602- G 025. F510 & V images overlayed with smoothed [O III]-line image contours.

NGC 7679

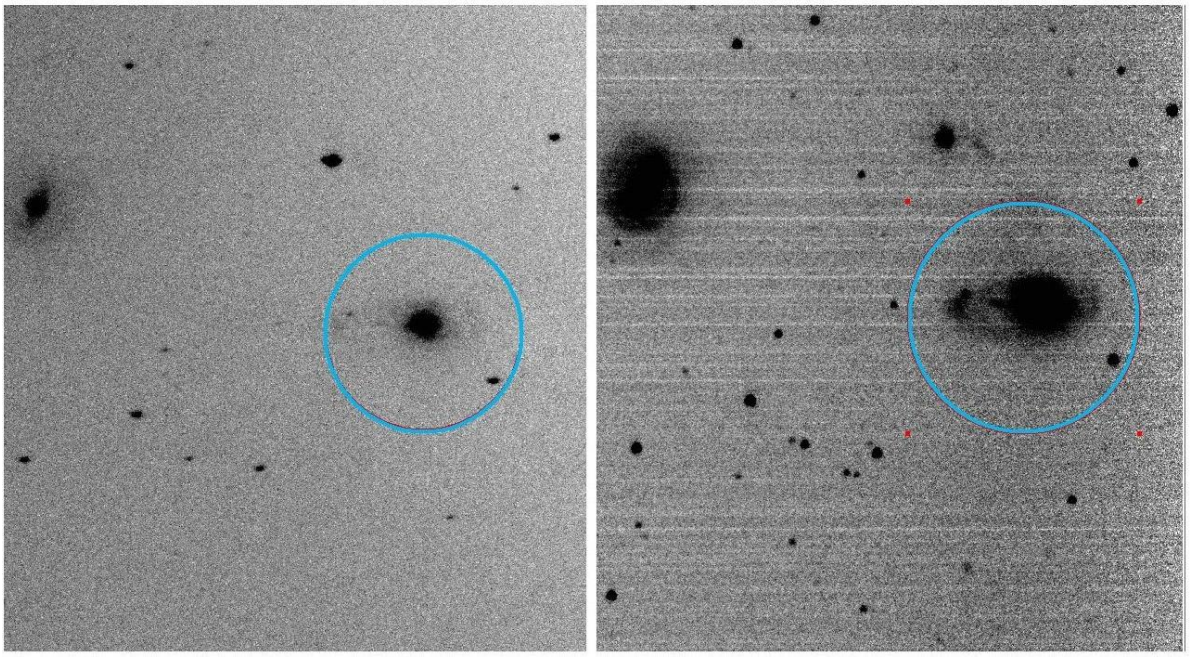

Figure 42: NGC 7679, F510 & V images

NGC 7682

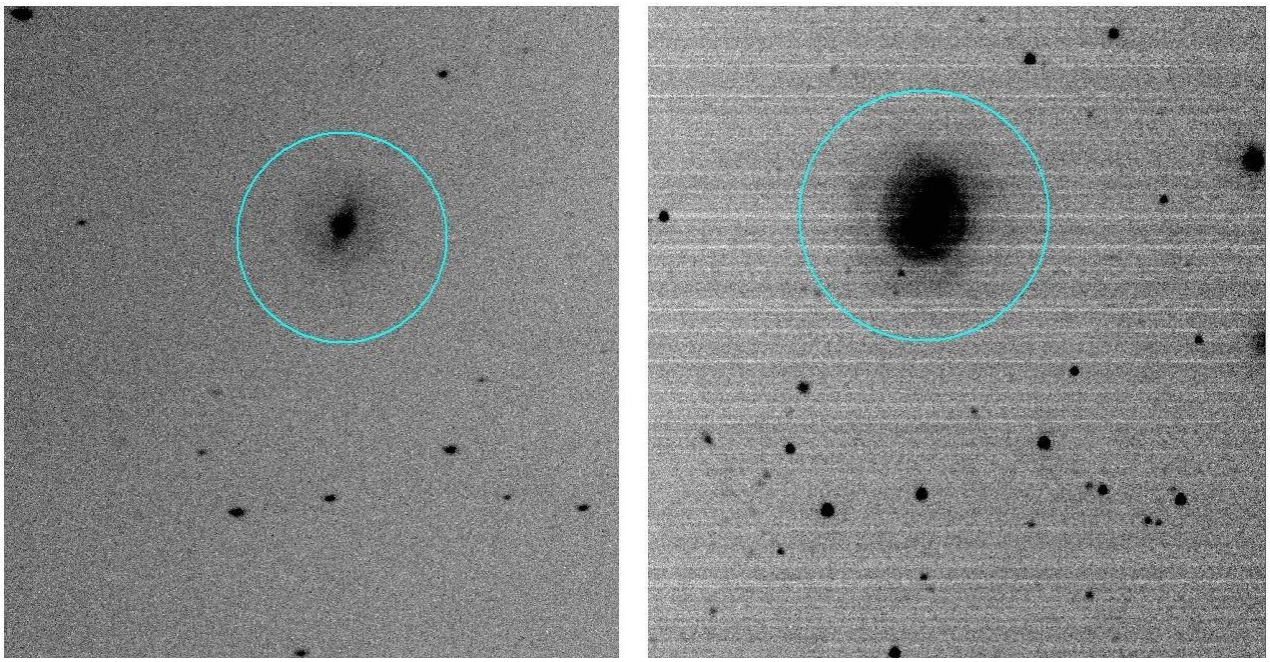

Figure 43: NGC 7682, F510 & V images

(1)	Name	(3) **f510** t(s), #	(4) **V** t(s), #
*	MARK 341	4800, 4	1320, 3
ag	Mrk 352	2700, 2	1000, 2
ag	Mrk 1	5400, 3	1200, 3
ag	NGC 513	5400, 3	1800, 3
N	Mrk 993	2400, 2	1020, 3
N	Mrk 359	2700, 2	900, 2
N	UGC 1395	4200, 3	1800, 3
*	NGC 841	2700, 2	1200, 2
N	Mrk 1040	2400, 3	1500, 3
ag	NGC 973	3600, 2	1200, 2
N	NGC 1167	3600, 2	1200, 2
*	UGC 3157	3600, 2	1200, 2
N	MS 04595+0327	3600, 2	1800, 3
*	2E 0507+1626	5400, 3	1800, 3
N	MCG -04.16.001	5400, 3	1800, 3
N	UGC 3478	3600, 2	1200, 2
N	UGC 3995	5400, 3	1800, 3
N	NGC 2639	3600, 2	1800, 3
*	NGC 2824	5400, 3	1800, 3
N	MCG -01.24.012	5400, 3	1800, 3
ag	Mrk 1419	5400, 3	1800, 3
Y	RXS J11032-0654	5400, 3	1800, 3
N	NGC 3822	5400, 3	1800, 3
N	NGC 4404	5400, 3	1800, 3
*	NGC 4619	3600, 2	1200, 2
N	3C 278	5400, 3	1800, 3
*	Mrk 461	5400, 3	1200, 2
N	IRAS 14082+1347	5400, 3	1800, 3
N	Mrk 1510	5400, 3	1200, 2
*	NGC 5548	7200, 4	1800, 3
ag	Zw 338.014	5400, 3	1800, 3
N	NGC 6240	5400, 3	1200, 2
N	Ark 539	5400, 3	1800, 3
N	UGC 11630	3600, 2	1800, 3
N	NGC 7469	3000, 3	1200, 2
ag	IC 1515	3600, 2	1200, 2
*	ESO 602-G25	2400, 2	900, 2
ag	NGC 7679	7200, 4	3600, 12
N	NGC 7682	7200, 4	3600, 12

Table 4. Column 1 indicates if emission line structures were detected: ag is used if structures were caused by afterglow effects and * indicates no obvious structure but more imaging is needed. Total exposure time in seconds and the number of exposures for the f510 (3) and V (4) filters are listed.

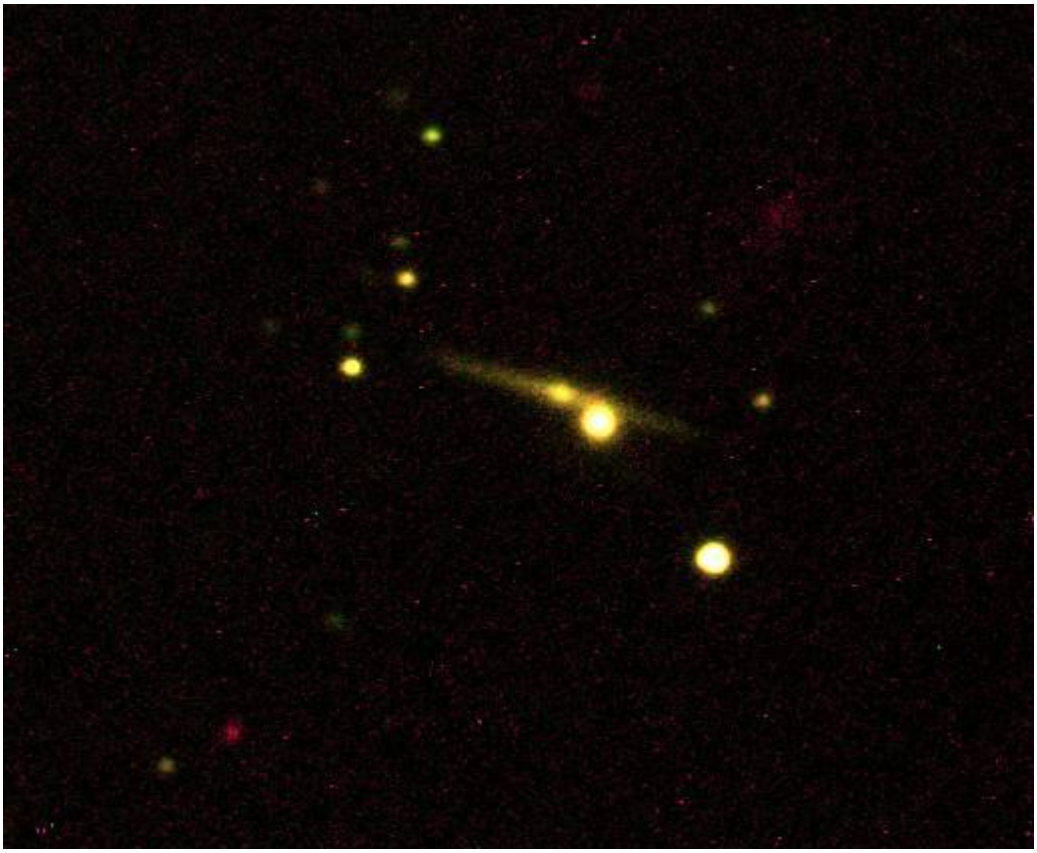

Fig. 44. RX J1103.2-0654. Color Combined [O III], V, and emission line image of RXS J11032-0654. This S1 galaxy overlaps a nearby disk galaxy. Emission clouds are red.

The only detection of diffuse ionized emission clouds in this study were found around the AGN RXS J11032-0654. Calibrated flux limits need to be calculated and additional useful data to acquire includes spectra and narrowband imaging in other emission lines. It is too early to speculate on the reasons why no emission clouds were detected around galaxies in the HI sample, since illuminated tidal debris is a candidate for the gas in extended emission line regions, though it could be that none happen to have an opening angle over which ionized

radiation comes out in a direction such that it can reach and ionize the extraplanar HI that we know is present.

The dramatic findings from Hanny's Voorwerp and the re-examination/search for extended ionized clouds it has prompted could place its discovery among the crucial and historic steps to understanding galaxy formation and the link to black hole accretion dynamics. The goal of this research was to search for Voorwerp analogues so that we may carry out further studies of those found to determine properties of their ionization source, presumably the nearest AGN. These further studies should include getting spectra and additional narrowband imaging. The SARA telescopes are equipped for Hαimaging over our redshift range, and so future SARA observations could determine the flux ratio [O III]-line/Hα. Since a recently faded AGN may not spectroscopically classify as such, a similar search to the one we've presented but around inactive galaxies is important and ongoing. Those results plus the future studies planned will be important for drawing general conclusions, which are not allowed by this work alone.

References

[1] R. Antonucci. Unified models for active galactic nuclei and quasars. *Annual review of astronomy and astrophysics*, 31:473–521, 1993.

[2] M. C. Begelman. A Nuclear Regula-Tori Model for Quasars and Seyferts. In R. Fanti, K. I. Kellermann, & G. Setti, editor, *VLBI and Compact Radio Sources*, volume 110 of *IAU Symposium*, pages 227–+, 1984.

[3] J. Binney and S. Tremaine. *Galactic Dynamics: Second Edition*, page 33. Princeton University Press, 2008.

[4] Richard D. Crisp. Residual bulk image: Cause and cure. *Sky & Telescope*, 121:72–75, May 2011.

[5] M. Dadina, M. Guainazzi, M. Cappi, S. Bianchi, C. Vignali, G. Malaguti, and A. Comastri. X-ray imaging of the ionisation cones in NGC 5252. *Astronomy and Astrophysics*, 516:A9+, June 2010.

[6] E. A. Fath. *The Spectra of Some Spiral Nebulae and Globular Star Clusters.* PhD thesis, University of California, Berkeley., 1909.

[7] H. Fu and A. Stockton. A Common Origin for Quasar Extended Emission-Line Regions and Their Broad-Line Regions. *The Astrophysical Journal Letters*, 664:L75–L78, August 2007.

[8] M. Fukugita, K. Shimasaku, and T. Ichikawa. Galaxy Colors in Various Photometric Band Systems. *Publications of the Astronomical Society of the Pacific*, 107:945–+, October 1995.

[9] G. I. G. et al. Josza. Revealing hanny's voorwerp: radio observations of ic 2497. *Astronomy and Astrophysics*, 500:133, 2009.

[10] William Keel. Introduction - discovery of active galactic nuclei. Website: http://www.astr.ua.edu/keel/agn/text.html.

[11] E. Y. Khachikian and D. W. Weedman. An atlas of Seyfert galaxies. *Astrophysical Journal*, 192:581–589, Sep 1974.

[12] J. H. Krolik. Magnetized Accretion inside the Marginally Stable Orbit around a Black Hole. *The Astrophysical Journal Letters*, 515:L73–L76, April 1999.

[13] C. Y. Kuo, J. Lim, Y. W. Tang, and P. T. P. Ho. Prevalence of tidal interactions among local seyfert galaxies. *Astrophysical Journal*, 679:1047–1093, June 2008.

[14] C. J. Lintott, K. Schawinski, W. Keel, H. van Arkel, N. Bennert, E. Edmondson, D. Thomas, D. J. B. Smith, P. D. Herbert, M. J. Jarvis, S. Virani, D. Andreescu, S. P. Bamford, K. Land, P. Murray, R. C. Nichol, M. J. Raddick, A. Slosar, A. Szalay, and J. Vandenberg. Galaxy Zoo: 'Hanny's Voorwerp', a quasar light echo? *Monthly Notices of the Royal Astronomical Society*, 399:129–140, October 2009.

[15] C. J. Lintott, K. Schawinski, A. Slosar, K. Land, S. Bamford, D. Thomas, M. J. Raddick, R. C. Nichol, A. Szalay, D. Andreescu, P. Murray, and J. Vandenberg. Galaxy Zoo: morphologies derived from visual inspection of galaxies from the Sloan Digital Sky Survey. *Monthly Notices of the Royal Astronomical Society*, 389:1179–1189, September 2008.

[16] J. Magorrian, S. Tremaine, D. Richstone, R. Bender, G. Bower, A. Dressler, S. M. Faber, K. Gebhardt, R. Green, C. Grillmair, J. Kormendy, and T. Lauer. The Demography of Massive Dark Objects in Galaxy Centers. *The Astronomical Journal*, 115:2285–2305, June 1998.

[17] Miller, J. S. and Antonucci, R. R. J. Evidence for a highly polarized continuum in the nucleus of NGC 1068. *Astrophysical Journal, Part 2 - Letters to the Editor*, 271:L7–L11, 1983.

[18] R. Narayan and I. Yi. Advection-dominated accretion: A self-similar solution. *The Astrophysical Journal Letters*, 428:L13–L16, June 1994.

[19] Prieto, M.A. and Freudlng, W. The relation between the neutral and the ionized gas in ngc 5252. *Monthly Notices of the Royal Astronomical Society*, 279:63–71, 1996.

[20] M. J. Rees. Emission from the nuclei of nearby galaxies - Evidence for massive black holes. In E. M. Berkhuijsen & R. Wielebinski, editor, *Structure and Properties of Nearby Galaxies*, volume 77 of *IAU Symposium*, pages 237–242, 1978.

[21] E. E. Salpeter. Accretion of Interstellar Matter by Massive Objects. *Astrophysical Journal*, 140:796–800, August 1964.

[22] K. Schawinski, D. A. Evans, S. Virani, C. M. Urry, W. C. Keel, P. Natarajan, C. J. Lintott, A. Manning, P. Coppi, S. Kaviraj, S. P. Bamford, G. I. G. Józsa, M. Garrett, H. van Arkel, P. Gay, and L. Fortson. The Sudden Death of the Nearest Quasar. *The Astrophysical Journal Letters*, 724:L30–L33, November 2010.

[23] M. Schmidt. 3C 273 : A Star-Like Object with Large Red-Shift. *Nature*, 197:1040–+, March 1963.

[24] C. K. Seyfert. Nuclear Emission in Spiral Nebulae. *Astrophysical Journal*, 97:28–+, January 1943.

[25] V. M. Slipher. The spectrum and velocity of the nebula N.G.C. 1068 (M 77). *Lowell Observatory Bulletin*, 3:59–62, 1917.

[26] A. Stockton, H. Fu, and G. Canalizo. QSO extended emission-line regions. *New Astronomy Reviews*, 50:694–700, November 2006.

[27] M.-P. Véron-Cetty and P. Véron. A catalogue of quasars and active nuclei: 13th edition. *Astronomy and Astrophysics*, 518:A10+, July 2010.

[28] W. C. Keel, S. D. Chojnowski, V. N. Bennert, K. Schawinski, C. J. Lintott, S. Lynn, A. Pancoast, C. Harris, A. M. Nierenberg, A. Sonnenfeld, R. Proctor. The Galaxy Zoo survey for giant AGN-ionized clouds: past and present black-hole accretion events. *Monthly Notices of the Royal Astronomical Society*, In press, 2011.